FEATURE ARTICLE

Molecular Studies of Catalytic Reactions on Crystal Surfaces at High Pressures and High Temperatures by Infrared−Visible Sum Frequency Generation (SFG) Surface Vibrational Spectroscopy

Gabor A. Somorjai* and Günther Rupprechter†

Department of Chemistry, University of California at Berkeley, and Materials Sciences Division, E. O. Lawrence Berkeley National Laboratory, Berkeley, California 94720

Received: September 15, 1998; In Final Form: December 31, 1998

Infrared−visible sum frequency generation (SFG) is a surface-specific vibrational spectroscopy that can operate in a pressure range from ultrahigh vacuum (uhv) to atmospheric pressures. SFG is therefore one of the few surface science techniques that permits atomic scale monitoring of surface species during catalytic reactions at high pressures (around 1 atm) and high temperatures. Using single-crystal surfaces of transition metals, platinum and rhodium, reaction rates can be simultaneously determined by gas chromatography, and correlations between the concentration of adsorbates under reaction conditions and the observed turnover numbers can help to elucidate the reaction mechanism. To bridge the gap to traditional surface science experiments, SFG is also employed under uhv or low pressures. The technique has been successfully applied to the adsorption and oxidation of CO, hydrocarbon conversion such as ethylene hydrogenation and cyclohexene hydrogenation and dehydrogenation on Pt(111). The experiments demonstrate that the key intermediates of high-pressure catalytic reactions are not present under low-pressure (uhv) conditions. Furthermore, the identification of active intermediates and their concentration at ambient conditions allows calculation of turnover frequencies per active surface species rather than simply per surface metal atom.

1. Introduction

Modern surface chemistry started with the use of single-crystal surfaces that could be characterized on the atomic scale.[1−5] The single crystals were usually small surface area (∼1 cm^2) samples that could be cleaned in ultrahigh vacuum (uhv) by ion bombardment and heating in chemically reactive gases. Defects introduced by these treatments were subsequently healed by annealing at high temperature. The surface structure and composition of the single crystals were determined by electron scattering and ion scattering techniques that could only be employed in a vacuum or at low pressures ($<10^{-4}$ mbar, 1 mbar = 100 Pa) because of the large mean free path that was necessary for the electrons or ions to reach the detector. Molecules could be adsorbed on these crystal surfaces, and their structures and bonding could be studied with the available techniques, for example, low-energy electron diffraction (LEED), Auger electron spectroscopy (AES), X-ray photoelectron spectroscopy (XPS), high-resolution electron energy loss spectroscopy (HREELS), and others.[6]

When high pressures were required to carry out catalytic reactions on these surfaces, uhv-compatible high-pressure reaction cells were connected to the uhv system.[7−10] The gas-phase analysis for kinetic measurements was performed by gas chromatography. Surface analysis had to be carried out in uhv before and after the high-pressure studies. These pre- and postreaction studies of the catalytically active surfaces were very informative. They revealed that the structure of the surface is often altered during the reaction. In many cases, the surface composition also changed dramatically by the reaction mixture that frequently deposited an overlayer that was tenaciously held to the metal crystal surface.[2,11]

Even low-pressure LEED surface crystallography studies have shown that adsorbed atoms and molecules cause restructuring of metal surfaces.[12−15] To optimize the adsorbate−metal surface chemical bond, the metal atoms relocate around the adsorption site. This is called *adsorbate-induced surface restructuring.*[2,16,17] The exothermic adsorption process compensates for the weakening of the metal−metal nearest-neighbor bonds that occur when metal atoms relocate around the adsorption site.

It became clear that it is necessary to carry out molecular level investigations of the surface *during* the chemical reaction and not just before and after the reaction. The surface restructuring in the presence of the high-pressure reactants and the nature of the adsorbed intermediates are likely to be very different during the high-pressure reaction from what is observed before or after a reaction in an analysis of surfaces in a vacuum or at low pressures (e.g., one would expect to see only strongly bound

* Corresponding author. Phone: (510) 642-4053. Fax: (510) 643-9668. E-mail: somorjai@socrates.berkeley.edu. http://www.cchem.berkeley.edu/∼gasgrp.

† Present address: Fritz-Haber-Institut der Max-Planck-Gesellschaft, Chemical Physics Department, Faradayweg 4-6, D-14195 Berlin, Germany. E-mail: rupprechter@fhi-berlin.mpg.de.

10.1021/jp983721h CCC: $18.00
Published on Web 02/20/1999

TABLE 1: Surface Science Techniques Most Frequently Used for Molecular-Level Studies at High Reactant Pressures

atomic force microscopy (AFM)[29,30]
calorimetry[31,32]
electron microscopy (using environmental cells) TEM[33,34]
electron paramagnetic resonance (EPR)[35,36]
extended X-ray absorption fine structure (EXAFS)[37]
Fourier transform infrared spectroscopy (FTIR)[38−40]
infrared reflection absorption spectroscopy (IRAS)[41−43]
isotope labeling[44]
Mössbauer spectroscopy[45,46]
Nuclear magnetic resonance (NMR)[47−49]
positron emission[50,51]
Raman spectroscopy[52−54]
scanning tunneling microscopy (STM)[17,55,56]
sum frequency generation (SFG)[27,57]
surface enhanced Raman spectroscopy (SERS)[58−60]
UV Raman spectroscopy[61,62]
X-ray diffraction (XRD)[63−65]

species under uhv since the weakly bound ones may desorb quickly).

In recent years, several surface science techniques are being developed that permit molecular level investigation of surfaces at high pressures during chemical reactions. A list of these techniques is shown in Table 1. Perhaps the most successful method for studying of single-crystal surfaces is sum frequency generation (SFG) surface vibrational spectroscopy.[18−22] It is based on a nonlinear optical phenomenon of laser spectroscopy that can lead to the summing of two photons of frequency ω_1 and ω_2. If $\omega_1 = \omega_2$, the process is called second harmonic generation. If one of the photons is at fixed frequency while the other photon's frequency is tuned, a vibrational spectrum can be obtained. SFG is uniquely surface monolayer specific because such a nonlinear process can only occur in media that do not possess inversion symmetry; the surface is such a medium, while the bulk of most solids and the gas phase do not give rise to the phenomenon.[23] Therefore, the vibrational spectrum originates mainly from the interface, unlike the circumstance encountered in infrared spectroscopy where the signals generated from the bulk and gas phase must be subtracted.

We have carried out systematic studies of adsorption and catalyzed reactions over metal single-crystal surfaces in a high-pressure environment, e.g., adsorption of gases at high pressures where the coverage is high, and catalytic reactions at high pressures. SFG often yields the vibrational spectra of adsorbates with about 1% of a monolayer sensitivity and with a 5 cm^{-1} energy resolution even at atmospheric pressures. This paper describes our findings obtained over the past 5 years [24−28] starting with the adsorption and oxidation of CO, followed by hydrocarbon conversion such as ethylene hydrogenation and cyclohexene hydrogenation and dehydrogenation.

If vibrational spectra of adsorbed molecules are recorded as a function of pressure *molecular adsorption isotherms* can be obtained. They reveal how the adsorbate structure changes as a function of coverage that is pressure dependent in equilibrium with the gas phase. We could also monitor the surface during catalytic reaction and determine which of the species turn over and are reaction intermediates and which are only spectators. Weakly adsorbed species that are reaction intermediates could be detected that would be absent from the surface at low pressures. Often, dehydrogenated molecules cover the surface during hydrogenation reactions and the nature of the molecular adsorbates changes with reactant pressure. Our studies indicate that the surface chemistry present at low pressures or in a vacuum cannot be readily extrapolated to predict the chemistry that occurs at high pressures and coverages.

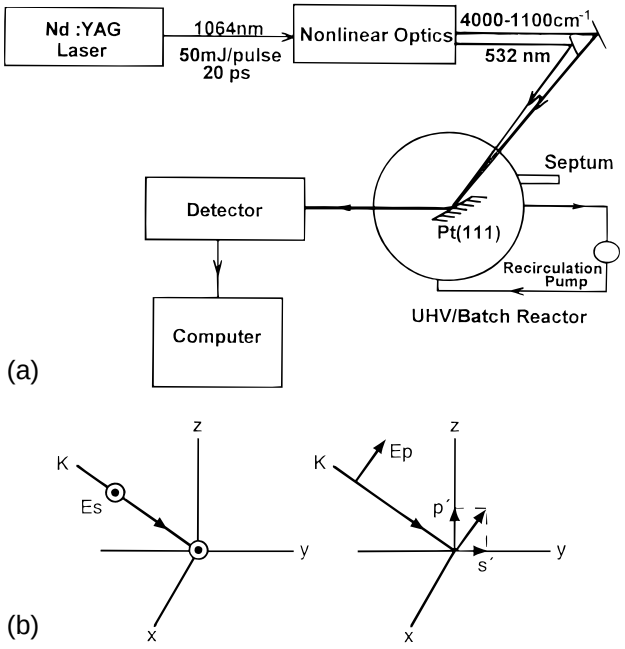

Figure 1. (a) Schematic of the uhv compatible batch reactor coupled to a Nd:YAG laser for in situ SFG studies. (b) Illustration of the polarization of incident beams.

2. Experimental Section

2.1. Sum Frequency Generation Process. Infrared−visible SFG is an *interface specific* vibrational spectroscopy technique that can be utilized to monitor chemisorption of molecules or their catalytic reactions over a 14 order of magnitude pressure range, from uhv up to several atmospheres. As a result of its surface specificity, it has been widely used in interfacial studies, and the SFG process has been reviewed in great detail in the literature.[19−23,66−72] It is a second-order nonlinear optical three-wave mixing process which involves the addition of infrared (ω_{ir}) and visible light (ω_{vis}) to produce light at the sum of these two frequencies ($\omega_{sf} = \omega_{ir} + \omega_{vis}$)[18,22] (Figure 1a). The process is only allowed (in the electric dipole approximation) in a medium without inversion symmetry (centrosymmetry). The lattice in the bulk of a, e.g., face-centered cubic (fcc), metal is centrosymmetric and, therefore, in the case of an adsorbed monolayer, the SFG signal is dominated by the contribution from the interface between the metal and vacuum. An isotropic gas phase also does not contribute to the signal.

To carry out an SFG experiment, the visible beam is held at fixed frequency while the infrared beam is tuned over the vibrational range of interest. As the IR beam is tuned through vibrational resonances of surface species, the effective surface nonlinear susceptibility $\chi_s^{(2)}$ is resonantly enhanced. The surface itself may also contribute to the signal, but the substrate response is nearly invariant and called nonresonant background. The SFG signal is proportional to the absolute square of $\chi_s^{(2)}$ ($|\chi_s^{(2)}|^2$), and hence, a vibrational spectrum of the surface species is detected. Formally, we can write

$$\chi_s^{(2)} = \chi_R^{(2)} + \chi_{NR}^{(2)} \quad (1)$$

and

$$\chi_R^{(2)} = \sum_q \frac{A_q}{\omega_{IR} - \omega_q + i\Gamma_q} \quad (2)$$

where $\chi_R^{(2)}$, $\chi_{NR}^{(2)}$, A_q, ω_q, ω_{IR}, and Γ_q refer to the resonant nonlinear susceptibility, nonresonant nonlinear susceptibility, strength of the qth vibrational mode, qth vibrational mode (resonant frequency), infrared laser frequency, and the damping constant of the qth vibrational mode, respectively. We can further write

$$A_q = \frac{1}{2\omega_q} \frac{\partial \mu_n}{\partial_q} \frac{\partial \alpha_{lm}^{(1)}}{\partial_q} \quad (3)$$

where μ_n is the dipole moment, $\alpha_{lm}^{(1)}$ is the linear polarizability tensor, and accordingly $\partial\mu_n/\partial q$ and $\partial\alpha_{lm}^{(1)}/\partial q$ are the infrared dipole derivative and the Raman polarizability change for the normal mode Q. Equation 3 clearly illustrates the selection rule for the SFG process. To be SFG active, a mode must be simultaneously infrared *and* Raman active. In a medium with inversion symmetry, the mutual exclusive law prohibits a mode to be both IR and Raman active; therefore, the lack of inversion symmetry is a prerequisite for SFG.

SFG can be carried out using different polarization combinations to gain information about molecular orientations (Figure 1b).[66,73] This method has been successfully applied to the characterization of polymer surfaces.[74] However, over metal surfaces the electric field of an s-polarized incident infrared beam is canceled out due to the image field of the electrons in the metal. An s-polarized beam can therefore not excite the dipole along the surface. While the s-polarized beam has only an s-component on the molecular frame, a p-polarized infrared beam is comprised of both s- and p-components (with the p-component not being canceled out). Accordingly, in SFG studies over metal surfaces, the infrared beam is always p-polarized. The visible beam can be both s- and p-polarized, but the signal from the (s-visible, p-infrared) combination is almost 40 times weaker than that from the (p, p) combination. Therefore, all experiments reported here were made in (p, p) geometry, which results in a p-polarized SFG output.

SFG has been proven to be a very powerful technique for surface spectroscopic investigations, but it also has a number of limitations. One of the drawbacks of SFG is its need for flat surfaces. Many studies were carried out on single-crystal surfaces, and results on Pt foil were published just recently.[75] Rough surfaces scatter the beams and only produce weak signal, and microporous materials cannot be studied. The high-power laser input (see below) may damage the sample surface. More and better nonlinear crystals are being developed, but there are still limitations in the accessible frequency range; wavenumbers below 1100 cm^{-1} are not readily accessible by SFG at present.

2.2. Laser System. The electromagnetic radiation for the experiment is generated by a passive, active mode-locked Nd:YAG laser which outputs a 20 ps pulse at 1064 nm when using #5 dye from Kodak (Figure 1a). The repetition rate of the laser is 20 Hz, and the total energy per pulse is about 50 mJ. The energy is divided into three portions, the first of which is frequency doubled from the 1064 nm Nd:YAG fundamental using a KD*P nonlinear crystal to produce green light at 532 nm. The remaining light is employed to generate infrared light by one of two angle tunable optical parametric generator/amplifier (OPG/OPA) stages capable of producing infrared radiation over the range from 1100 to 4000 cm^{-1}. The first OPG/OPA generates light from 2500 to 4000 cm^{-1} with fwhm of 12 cm^{-1} at 2880 cm^{-1} using $LiNbO_3$, while the second β-BaB_2O_4-(BBO) OPG/OPA is angle-tunable from 1100 to 2500 cm^{-1} with a fwhm of 4 cm^{-1} by difference frequency generation in a $AgGaS_2$ crystal.[76] The infrared and visible beams are temporally aligned and focused concentrically on the metal catalyst inside the batch reactor. Both the green and IR light used in this experiment were p-polarized such that their electric fields had components perpendicular to the surface of the platinum crystal (Figure 1b). The spot diameter of the green beam is approximately 1.5 mm at the sample, and the beam makes an angle of 50° with respect to the surface normal. The input energy is about 400 μJ. These values yield a total power of approximately 1 GW/cm^2. This regime has been shown experimentally to be at least a factor of 4 below powers that either cause photochemistry or damage the platinum sample even over extended periods of time. The infrared radiation is focused to approximately 1.2 mm inside the green spot at an angle of 55° with respect to the surface normal, and the maximum energy out of the OPG/OPA is always used. The infrared power varies widely with frequency. The maximum infrared power is at 2850 cm^{-1}. At this frequency, the IR energy at the sample is approximately 275 μJ/pulse when using Kodak #5 dye, while the energy drops to about 20 μJ around 1200 cm^{-1}.

The difference in the incident angles of the beams is necessary to spatially separate the SFG signal from the reflected pump beams. The blue (450−490 nm) sum frequency output from the sample crystal was collected by a photomultiplier tube and the signal sent to a gated integrator (after passing through a polarizer, filters, and a monochromator to remove all 532 nm contributions). A vibrational spectrum of surface species is obtained by monitoring the sum frequency signal as a function of the incident infrared photon energy. As mentioned earlier, for a vibrational mode to be observable by SFG, it must be both infrared and Raman active. Only those modes which lack centrosymmetry can in the dipole approximation simultaneously obey both rules. Therefore, in the experiments described in this paper, the isotropic gas phase and the fcc lattice of the bulk platinum sample possess inversion symmetry and give nearly zero contribution to the signal. Therefore, the dominant contribution is generated by the modes of the adsorbed monolayer at the platinum surface, where inversion symmetry is always broken.[77]

2.3. Reaction Chamber. High-pressure catalytic studies on Pt(111) were carried out in a uhv-batch reactor system which has been described in more detail elsewhere (Figure 1).[27] The reactor was equipped with CaF_2 windows to allow infrared and visible light to enter and to allow sum frequency light to exit to a photomultiplier tube. Sum frequency spectra were generally taken in the pressure range from 10^{-10} Torr to about 770 Torr (1 Torr = 133 Pa). Gases were introduced via a manifold, and high gas pressures were measured with a Baratron gauge. The gas was mixed by a recirculation pump, and the recirculation loop contained a septum for gas analysis by gas chromatography. The mixing time of the chamber was approximately 3 min as determined by following the dilution of a pulse of methane into a background of pure Ar. The reactor volume was 62.5 L and could be pumped out to a base pressure below 1×10^{-10} Torr by opening a gate valve to an ion and turbomolecular pump. The Pt(111) crystal used in the experiments was spot welded onto the manipulator with tantalum wires and was capable of being resistively heated to above 1200 K and cooled to 115 K under vacuum using liquid nitrogen (250 K under ambient pressure). Temperature was measured with a Chromel−Alumel thermocouple which was positioned on the edge of the crystal.

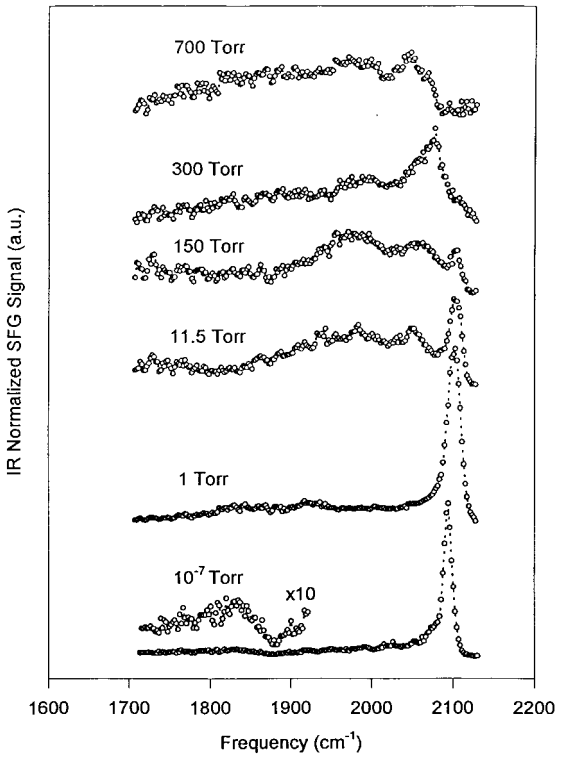

Figure 2. Pressure dependence of SFG spectra for CO adsorbed on Pt(111) at 295 K.

The chamber was also equipped with a Varian retarding field analyzer (RFA), for Auger and LEED, and a VG SX300 mass spectrometer. An Ar^+ gun could be used to remove undesirable impurities from the crystal surface. The large volume of the reactor limits our studies to reactions with turnover frequencies of at least 0.1 turnovers per site per second. We have therefore designed a new SFG-compatible uhv high-pressure cell with a volume 250 times smaller than that of the reaction cell used for the experiments described below. A description of the new cell will be presented in a forthcoming publication.[78]

2.4. Sample Preparation. The Pt(111) single crystals used in our experiments were circle-shaped disks, about 1 mm thick and up to 10 mm in diameter. They were cut from a 5N single-crystal boul (Goodfellow, UK) after orientation by Laue X-ray back-diffraction and polished by standard mechanical methods until X-ray back-diffraction showed a plane surface oriented to within 0.5° of the ⟨111⟩ direction. The single crystals were then cleaned in uhv by repeated cycles of Ar^+ ion bombardment and annealing at temperatures up to 1200 K until no more impurities could be detected by AES. The same treatments were used before and after every experiment (unless otherwise noted).

3. Chemisorption and Catalytic Reactions Studied In-situ by SFG

3.1. Carbon Monoxide Adsorption and Surface Restructuring. SFG studies of carbon monoxide adsorption on Pt(111) between 10^{-10} and 700 Torr revealed pronounced changes in the vibrational spectrum of the surface species, particularly at high CO pressures. The vibrational signatures of the adsorbed surface species indicate the formation of carbonyl−platinum cluster analogues that are coadsorbed with an incommensurate CO overlayer.

Figure 2 shows the SFG spectra of CO obtained at 295 K at various pressures. After exposing the clean Pt(111) surface to 10 langmuirs (1 langmuir = 10^{-6} Torr sec) of CO in uhv, two peaks at 1845 and 2095 cm^{-1} were observed which are characteristic of CO adsorbed at bridge and atop sites. The LEED pattern corresponded to a c(4 × 2) structure in which an equal number of CO molecules occupied atop and bridge sites.[79] This is in agreement with previous HREELS[80] and reflection−absorption infrared spectroscopy (RAIRS)[81] studies. The higher relative intensity of atop-bonded CO versus bridge-bonded CO results from the specific selection rule for the SFG process.[82] As mentioned earlier, SFG requires a vibrational mode to be simultaneously IR and Raman active so that the SFG intensity includes contributions from the Raman polarizability as well as the IR selection rule for the normal mode.

Upon increasing the pressure to 1 Torr, the frequency of atop species shifted to a higher value (2105 cm^{-1}) and the bridge-bonded CO disappeared. The frequency shift results from the enhancement of the dipole coupling between CO molecules on the surface because of their closer packing at high pressure, thereby weakening their bonds to the metal.[83] Surprisingly, by further increasing the pressure to 11.5 Torr, the intensity of the atop CO was attenuated without further frequency shift or broadening. At the same time, two new features at 1980 and 2045 cm^{-1} became visible. At 150 Torr of CO and higher (a pressure region that is not readily accessible to HREELS and IR spectroscopy), a broad peak covering 1980 and 2045 cm^{-1} features appeared and extended to 1800 cm^{-1} with a monotonic decrease of the intensity. At 700 Torr of CO, the spectrum was dominated by the new features and a strong background extended to 1700 cm^{-1} again with a monotonic decrease in intensity. All spectra were completely reversible and reproducible with variation of the gas pressure.[84]

Raising the carbon monoxide pressure caused the adsorption of more CO on the Pt(111) surface and, hence, a compressed overlayer was formed. This increased the repulsive interaction between CO as judged by the rapidly declining heat of adsorption with coverage.[85] However, under pressure, the interactions between CO molecules and platinum atoms are strong enough to overcome the CO−CO repulsion. The carbon monoxide molecules on the surface lost their registry of sites and formed an incommensurate overlayer as lower symmetry locations were occupied. Indeed, the strong background seen in the 1800−1980 cm^{-1} frequency range was the result of the formation of an incommensurate overlayer due to the ambiguity of site occupation. This explanation was further corroborated by high-pressure STM studies.[55]

The frequency of the 2045 cm^{-1} adsorption peak is characteristic of terminally bonded CO (Pt−CO) molecules; therefore, one reasonable explanation could be that atop CO has been squeezed out of its normal site and this has caused the frequency to shift to the lower value. The intensity of atop CO decreased with increasing pressure, while the 2045 cm^{-1} feature intensity went up. Another interpretation of the 2045 cm^{-1} peak is the multiple bonding species formation. The frequency is comparable to the vibrational frequency of terminally bonded CO in platinum carbonyl binary complexes $Pt-(CO)_n$ ($n = 1, 2, 3, 4$) synthesized by Ozin et al. by cocondensation of platinum atoms with carbon monoxide molecules in an argon matrix at very low temperature.[86] We favor the assignment of this peak to the multiple bonded platinum carbon monoxide cluster analogues on the surface. In our case, these cluster analogues were affected by the platinum substrate underneath, so the CO vibrational frequency is slightly red-shifted from Ozin's binary complexes.

The spectra at elevated CO pressure were consistent with earlier results showing CO chemisorption is accompanied by displacive reconstruction (i.e., distortion or relaxation of the

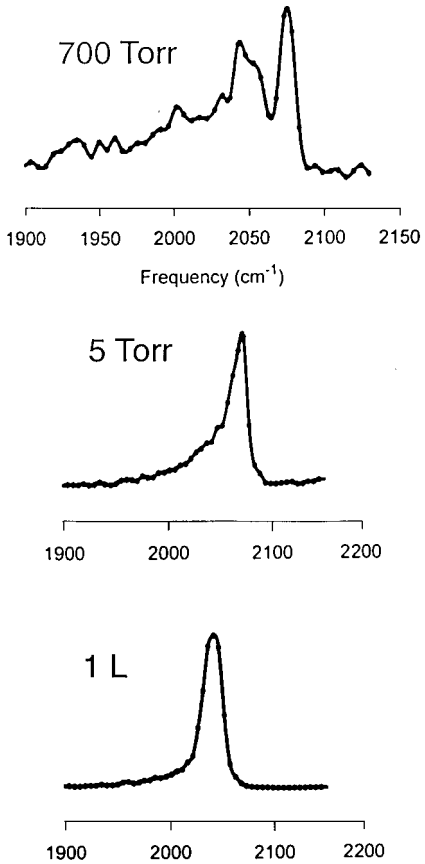

Figure 3. Pressure dependence of SFG spectra for CO adsorbed on Rh(111) at 295 K.

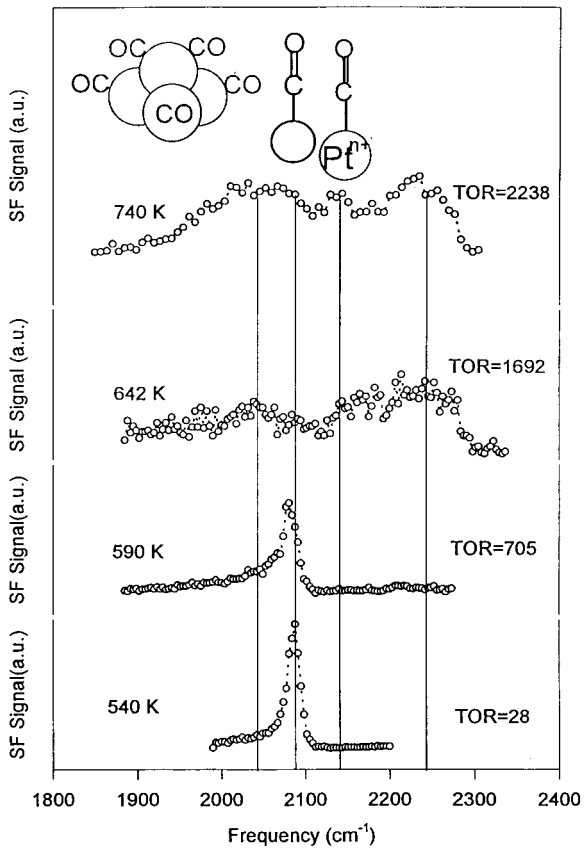

Figure 4. Temperature dependence of SFG spectra observed during high-pressure CO oxidation over Pt(111) at 40 Torr CO and 100 Torr O_2. The temperature and turnover rate are indicated.

transition metal surface).[87] In this model, some of the Pt atoms are pulled out from the crystal lattice, perhaps at a step or kink site, and become more exposed to the adsorbing CO molecules, thereby forming multiple bonded CO platinum complexes ($Pt_m(CO)_n$ with $n/m > 1$) or carbonyl analogues. However, at low pressure, because of the repulsive interaction of CO ligands, these complexes are not stable. They can only exist on the surface in the presence of high CO pressure. Most catalytic reactions require high reactant pressures, in the range of stabilization for the cluster-like species. As will be described below, our SFG studies during CO oxidation on the Pt(111) crystal face indicated the CO vibrational spectrum to be characteristic of the cluster-like species.

The room-temperature adsorption of CO has also been studied on Rh(111) in the range uhv to 1 atm.[88] After an exposure of 1 langmuir (5×10^{-8} Torr for 20 s), the SFG vibrational spectrum showed a single feature at 2042 cm^{-1}, which is the top site CO adsorption peak (Figure 3). Higher exposures induce a CO−CO coupling and blue shift this feature to 2068 cm^{-1}. Upon increasing the CO pressure to 700 Torr, a second peak appeared at slightly lower frequency (around 2040 cm^{-1}). We assigned this high-pressure peak to a top site CO on a roughened Rh(111) surface (according to its increased intensity on a nonannealed (defective) Rh(111) surface). The 2040 cm^{-1} peak disappears after the CO is pumped out, indicating that the surface roughening is reversible. This is consistent with our recent STM results. While Pt carbonyls are stable enough to allow their observation on the metal surfaces, Ni and Fe carbonyls, for instance, are volatile and their formation would lead to etching of the metal surface (the facile volatilization of $Ni(CO)_4$ is utilized to produce pure Ni in the Mond process).

3.2. Carbon Monoxide Oxidation on Pt(111). Carbon monoxide oxidation was carried out at various CO to oxygen ratios at a total pressure of 1 atm (with helium used as fill-up gas). The CO pressure was varied from tens to hundreds of Torr. The order in which CO and O_2 were introduced did not influence the results. The SFG spectra obtained during CO oxidation at different platinum crystal temperatures (with an initial condition of 40 Torr of CO and 100 Torr of O_2) and the measured turnover rates are displayed in Figure 4.

When the sample temperature was low, the reaction rate was low and the SFG spectrum was dominated by CO adsorbed at atop sites. With increasing temperature, the atop CO intensity decreased due to the thermal desorption of carbon monoxide and the reaction accelerated. At 540 K, a reaction rate of 28 molecules of CO_2/platinum surface site/second was obtained. When the crystal temperature increased to above 600 K, the reaction became self-sustained, proceeding at a constant high temperature without the need of heating because of the high exothermicity of this oxidation. The temperature at which the reaction becomes self-sustaining is defined as the ignition temperature. The ignition temperature is a function of the CO partial pressure; this dependence is shown in Figure 5.

The SFG spectra obtained at temperatures above ignition are significantly different from those obtained in the low-temperature regime. Atop CO, which is the dominant feature in the low-temperature regime, disappeared completely above ignition temperature, while there were three new features at 2050, 2130, and 2240 cm^{-1} that showed up as the turnover rate increased rapidly to 2238 molecules/platinum site/second. The 2130 cm^{-1} peak was assigned to the stretch mode of carbon monoxide adsorbed on the oxidized platinum sites, which has been shown not to be important in CO oxidation.[89] The broad peak centering at 2050 cm^{-1} and extending to 1700 cm^{-1} was assigned to new CO species, presumably multiple bonded platinum carbon

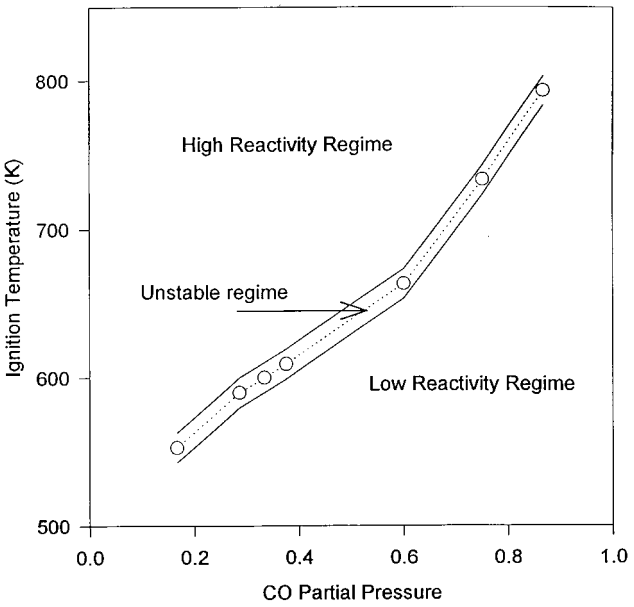

Figure 5. CO partial pressure dependence of the ignition temperature of CO oxidation over Pt(111).

monoxide cluster analogues and an incommensurate CO overlayer (cf. section 3.1).

The assignment of the feature at ~2240 cm^{-1} is difficult to make because the frequency is too high to be readily assigned to any of the surface CO species, since the frequency of the CO stretch mode in the gas phase is only 2143 cm^{-1}. Consequently, because of the frequency regime and the presence and the formation of carbon dioxide species on the surface, this feature could be assigned to a surface CO_2 related species. However, such a high frequency CO stretch has been reported when the molecule is bound to positively charged platinum.

In the presence of excess CO (at 100 Torr CO and 40 Torr O_2, for example), the vibrational spectrum became considerably simpler (Figure 6). The spectral features we assign to CO adsorption at an oxidized Pt site, and the one at 2240 cm^{-1} disappeared. Only the peaks associated with the presence of incommensurate and terminal CO species were detectable under these conditions.

The kinetics of CO oxidation changed with the change of the surface vibrational spectrum. Different apparent activation energies were observed for the two different temperature regimes, below and above ignition temperature. An activation energy of 175 kJ/mol was obtained for the low-temperature regime below ignition temperature, which is similar to the CO desorption energy. Above ignition temperature, where the reaction is self-sustained, a value of 58 kJ/mol was observed in the high-temperature regime (>600 K), which is close to the activation energy of 49 kJ/mol obtained in molecular beam studies.[90]

A correlation was also shown between the reaction turnover rate and the coverage of the surface CO species. In Figure 7a, the turnover rate at a constant temperature of 590 K is plotted as a function of the relative coverage of atop CO. The coverage was altered by changing the CO/O_2 ratio and was normalized to the low-temperature SFG intensity of the same species. With the decrease of atop CO coverage, the reaction rate increased greatly, indicating that atop CO is not a key intermediate during CO oxidation. Its presence on the surface inhibits the CO oxidation reaction. However, the reaction rate was proportional to the concentration of the surface CO species centered at 2050 cm^{-1} (Figure 7b), which is strong evidence that this species is

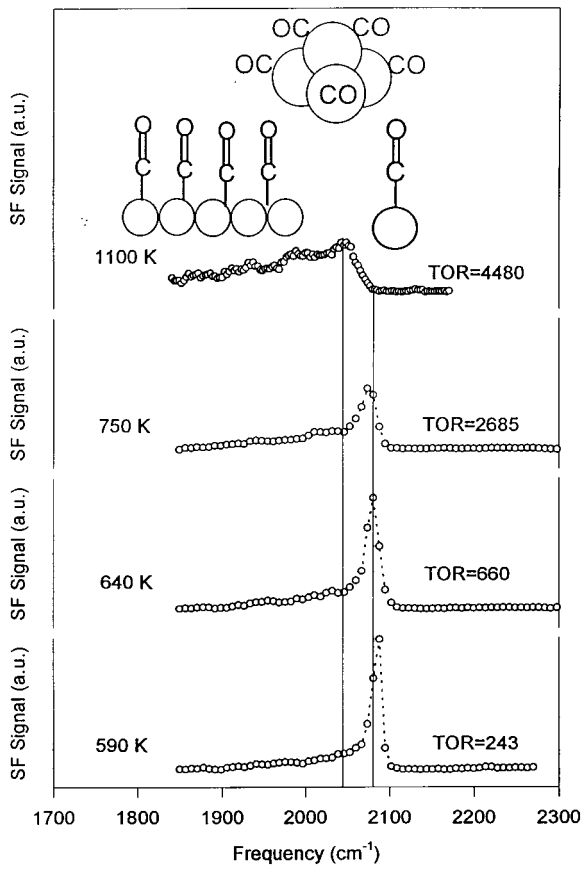

Figure 6. Temperature dependence of SFG spectra of high-pressure CO oxidation over Pt(111) at 100 Torr CO and 40 Torr O_2. The temperature and turnover rate are indicated.

active for oxidation to CO_2. Approximately half order dependence on both oxygen and carbon monoxide was found in the high-temperature regime above ignition temperature. It is well-known that this reaction has a negative order in CO at low temperature.

Summarizing, there were two different reaction regimes for CO oxidation over Pt(111) in the investigated temperature range. In the low-temperature regime (below ignition temperature), atop CO dominated the surface and the reaction has an activation energy of 175 kJ/mol. The reaction rate was inversely proportional to the surface concentration of atop CO. It appears that the atop CO inhibits the reaction by preventing oxygen from adsorbing on Pt(111). Below ignition, the desorption of atop CO seems to be the rate-limiting step. Above ignition temperature, new CO species (incommensurate overlayer and CO terminally bonded at distorted platinum sites) were dominant, and in excess oxygen, CO adsorbed on oxidized Pt. The reaction rate increased linearly with the surface concentration of the new CO species in the high-temperature regime (>600 K), indicating the active role of these CO species in CO oxidation.

3.3. Olefin Hydrogenation (Ethylene, Propylene, and Isobutene) on Pt(111). Our SFG studies of light olefin hydrogenation revealed that the π-bonded species of ethylene, propylene, and isobutene are the dominant intermediates which subsequently hydrogenate to alkanes at 300 K and atmospheric pressures. Other species that are present during this fast catalytic reaction, the strongly chemisorbed ethylidyne, propylidyne, and butylidyne and the corresponding di-σ-bonded species, are spectators that hydrogenate much too slowly to be important sources of the hydrogenated products. The π-bonded reaction intermediates are generally present in a concentration of a few

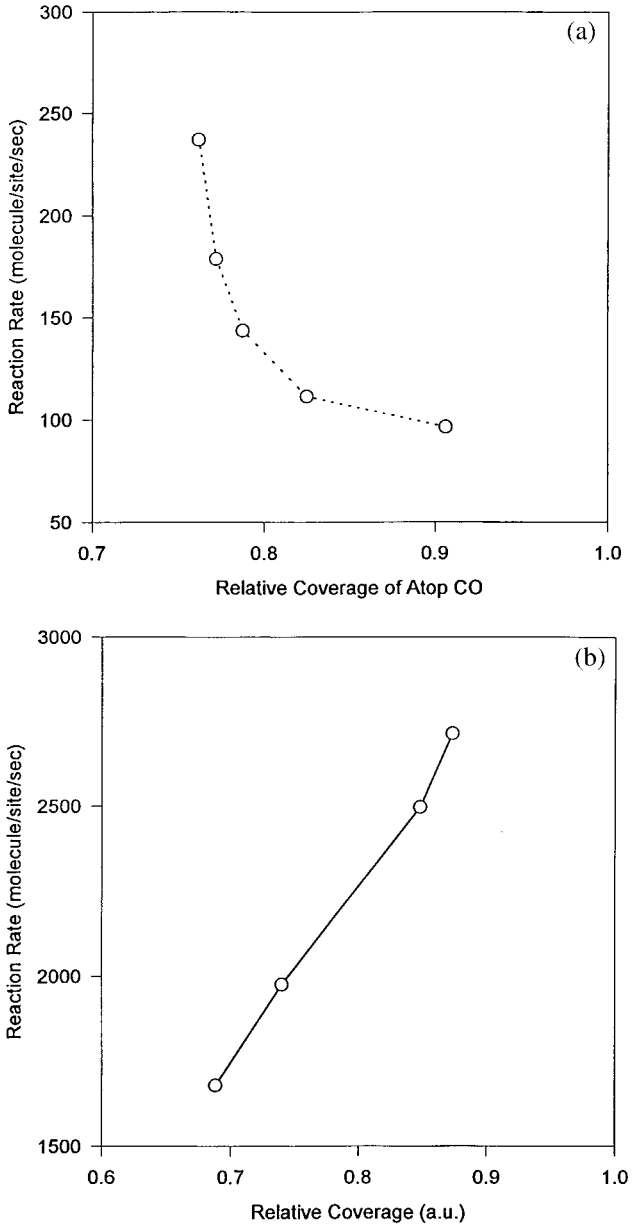

Figure 7. (a) Plot of the reaction rate as a function of atop CO coverage at 590 K. (b) Reaction rate as a function of the new CO species surface concentration at 720 K.

percent of a monolayer and are desorbed as the reactant pressure is decreased, indicating relatively weak surface bonding.

Ethylene hydrogenation on platinum is a simple catalytic reaction that readily occurs at room temperature. A reaction mechanism proposed by Horiuti and Polanyi [91] suggests that ethylene is hydrogenated stepwise by H atoms on the surface. In the absence of hydrogen, several distinct species have been identified in uhv conditions for a monolayer of ethylene absorbed on Pt(111). At temperatures below 50 K, monolayer molecules interact weakly with the surface via π-coordination. The molecule's π orbital bonds directly with the platinum surface with its C−C bond parallel to the surface. The interatomic distance between the two carbon atoms is almost unchanged with respect to the gas-phase molecule and this species is hence called π-bonded ethylene. At temperatures between 60 and 240 K, the carbon−carbon double bond of the gas-phase molecule is broken and the carbon atoms attain nearly sp^3 hybridization. Two σ bonds are formed with the underlying platinum surface atoms and this species is usually referred to as di-σ-bonded ethylene. Higher temperatures induce dehydrogenation of ethylene molecules. Ethylidyne is formed by losing one hydrogen and transferring a second hydrogen atom to the other carbon. Ethylidyne is the prevalent hydrocarbon species on the surface up to 450 K and resides in the fcc 3-fold hollow site.

The hydrogenation reaction intermediates have been studied by several groups using infrared spectroscopy,[92,93] but these experiments were carried out in the absence of ethylene in the gas phase. By contrast, SFG allows us to monitor the surface in situ under catalytic conditions.[25] The turnover rate (TOR) of ethylene hydrogenation on Pt(111) at 295 K with 35 Torr C_2H_4 and 100 Torr H_2 as determined by gas chromatography is 11 ± 1 ethylene molecules converted to ethane per platinum atom per second. Three features were present on the surface under these conditions at 2880 cm^{-1}, 2910 cm^{-1}, and a small peak around 3000 cm^{-1} (Figure 8a). Compared with fingerprint spectra of surface species prepared in a vacuum, the largest peak in the vibrational spectrum at 2880 cm^{-1} is the $\nu_S(CH_3)$ of ethylidyne (M≡CCH_3). The feature at 2910 cm^{-1} results from the $\nu_S(CH_2)$ of chemisorbed di-σ-bonded ethylene. The small peak just below 3000 cm^{-1} is the $\nu_S(CH_2)$ of (weakly bonded) physisorbed π-bonded ethylene. The weak $\nu_S(CH_2)$ signal for π-bonded molecules can be attributed to the surface-dipole selection rule for metal surfaces: dynamic dipoles parallel to the surface plane are canceled by image dipoles inside the metal (in addition, the concentration of π-bonded ethylene is small, as will be discussed below). The spectrum was stable for hours while the reaction rate remained constant. After the gas mixture was evacuated from the reactor, the surface was saturated with ethylidyne, while di-σ- and π-bonded ethylene molecules disappeared (Figure 8b). After the reaction cell was recharged with an ethylene/H_2 mixture, the reaction rate recovered (Figure 8c) and π-bonded ethylene was restored on the surface, while the intensity from the di-σ species did not return. This demonstrated a direct competition for adsorption sites between the ethylidyne and the di-σ ethylene. Since a high turnover rate was again observed in the second run in absence of di-σ-bonded species, the hydrogenation through the di-σ ethylene is at most a minor channel in the reaction scheme.

It was also observed that the ethylene hydrogenation reaction occurred at the same rate regardless of the presence of ethylidyne on the surface. Beebe et al.[94] and Rekoske et al.[93] monitored ethylene hydrogenation over Pd/Al_2O_3 and Pt/Cab-O-Sil supported catalysts by in situ transmission infrared spectroscopy. By varying the ratio of ethylene to H_2 it was shown that hydrogenation occurred both with and without an ethylidyne overlayer. In addition, preadsorbed ethylidyne groups do not affect the reaction rate. This indicates that ethylidyne is not directly involved in the hydrogenation reaction. The same conclusion was reached from a study of ^{14}C ethylidyne hydrogenation in hydrogen.[95] In contrast to the behavior of di-σ-bonded ethylene and ethylidyne, the appearance of π-bonded species is directly correlated with the reaction rate. It is most likely the key intermediate in ethylene hydrogenation. It should be emphasized that the other surface species present, di-σ-bonded ethylene and ethylidyne, are spectators and do not contribute to the turnover rate in any significant way.[27] It should further be noted that only these strongly chemisorbed species are normally detectable by studies in uhv, while the weakly bond π-bonded ethylene is more readily found at atmospheric reaction conditions. Surface ethyl groups are visible at very high hydrogen pressures. Under 727 Torr H_2 and 60 Torr C_2H_4 at 295 K, two additional peaks are present in the SFG spectrum

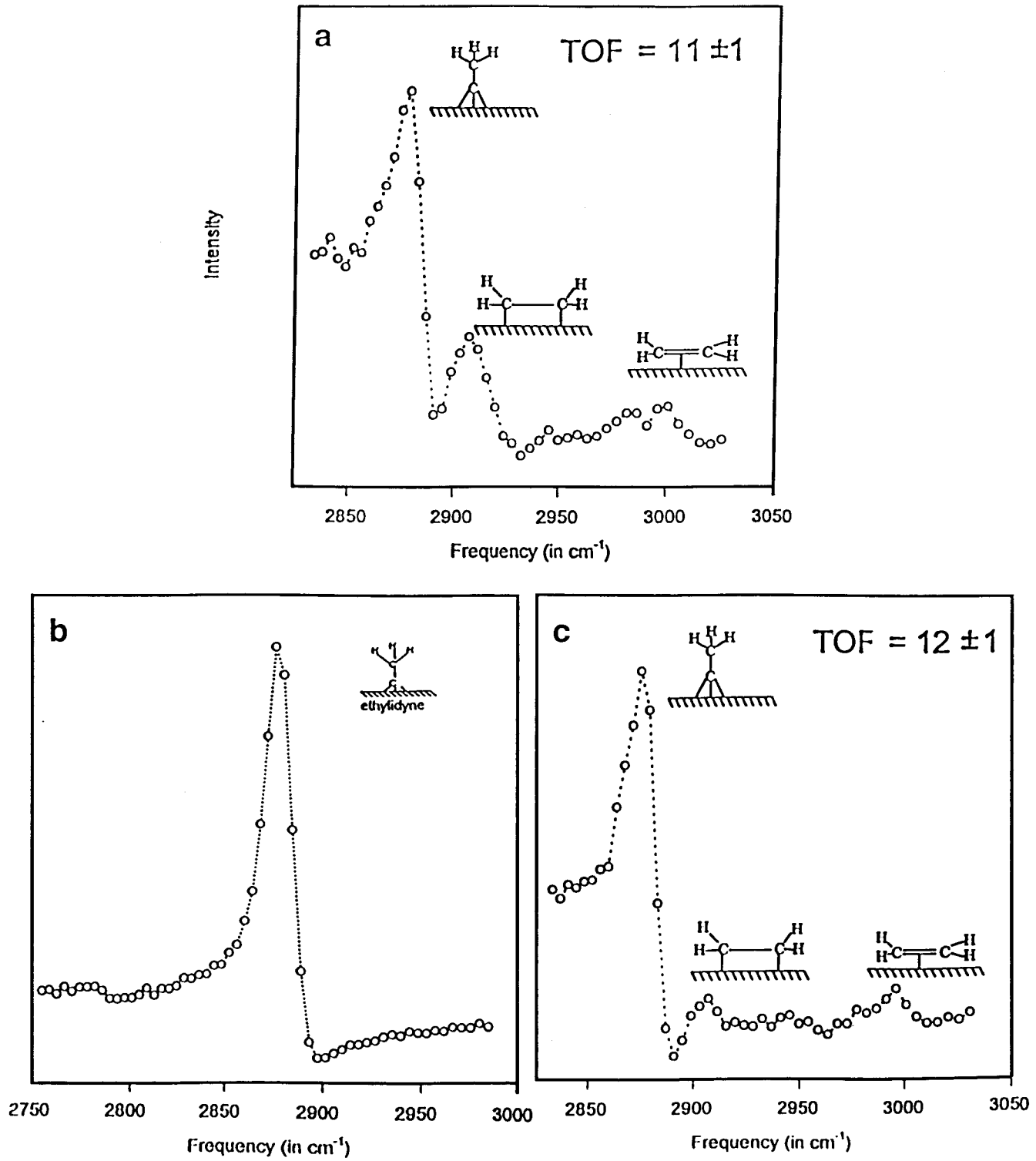

Figure 8. (a) SFG spectrum of the Pt(111) surface during ethylene hydrogenation with 35 Torr C_2H_4, 100 Torr H_2, 615 Torr He at 295 K. (b) Vibrational spectrum of the same system after the evacuation of the reaction cell. (c) SFG spectrum under the same conditions as (a), but on a surface which was precovered in uhv with 0.52 monolayers of ethylidyne.

which can be assigned to an ethyl species on the surface. The low surface concentration of ethyl groups at medium hydrogen pressure suggests a high degree of reversibility of the addition of the first hydrogen into adsorbed ethylene.

To determine the concentration of π-bonded ethylene on Pt(111) under reaction conditions, the peak intensity was calibrated by uhv spectroscopic measurements. The calibration was achieved by exposing the clean Pt(111) surface to a near-saturation coverage of oxygen at room temperature, followed by exposure to ethylene at 120 K.[96] This results in a mixture of π-bonded and di-σ-bonded ethylene on the surface at a concentration of 6% of a monolayer and 10% of a monolayer, respectively.[97] Using this spectrum as a reference, the intensity of the 3000 cm^{-1} peak corresponded to approximately 4% of a monolayer of reactive π-bonded ethylene. This means that the turnover rate for ethylene hydrogenation *per reactive intermediate species* is actually 25 times faster than per exposed platinum atom. Therefore, the absolute turnover rate of physisorbed ethylene is approximately 275 ethane molecules formed per surface intermediate per second under the above conditions.

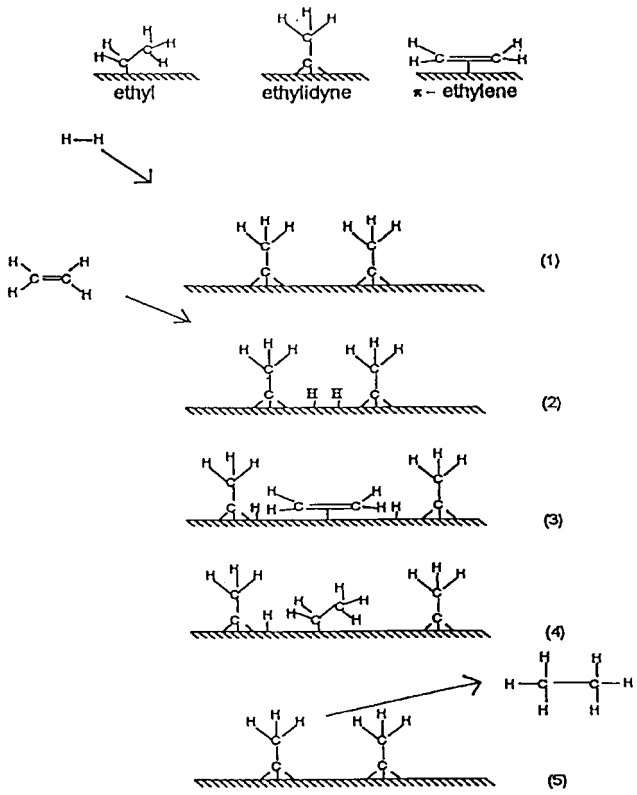

Figure 9. Proposed mechanism for ethylene hydrogenation on Pt(111).

The concentration of surface intermediates is too high for this reaction to be dominated by defects. In fact, it has been demonstrated that the rate of ethylene hydrogenation is independent of the platinum surface structure over which the reaction takes place (a so-called structure insensitive reaction).[98] Evidence from inorganic cluster analogues and homogeneous catalysis suggests that the reaction probably occurs on atop sites.[27] Hydrogenation at such sites leads to a structure insensitive reaction, because they are available on all crystal faces. The concentration of surface intermediates is much lower than one intermediate per surface platinum atom and remains constant at approximately 4% of a monolayer over a wide range of ethylene pressures. Therefore, this represents saturation coverage of π-bonded ethylene under reaction conditions, consistent with the kinetics of ethylene hydrogenation which are nearly zero order in ethylene partial pressure above approximately 25 Torr of C_2H_4.[99] It has been observed that ethylene hydrogenation is unaffected by decomposition species present on the surface during reaction.[94,95] Because the concentration of reaction intermediates is only 4% of a monolayer and the saturation coverage for the decomposition species, ethylidyne, is only 25% of a monolayer, it appears that there should always be sufficient sites available on which the reaction may occur.

We therefore propose a model in which π-bonded ethylene adsorbs on atop sites where it can be hydrogenated to ethane in the presence of mechanistically unimportant decomposition species. Figure 9 shows a schematic representation of the hydrogenation process. LEED surface crystallography studies determined that both ethylidyne and di-σ-ethylene species occupy 3-fold, face-centered cubic adsorption sites.[100] After these strongly adsorbing sites are occupied, π-bonded ethylene adsorbs at atop sites. In the process, the ethylidyne species may change location by moving from fcc to hcp 3-fold sites to leave more space for the π-bonded species. The rapid motion of ethylidyne at 300 K is indicated because the molecule cannot be imaged by STM, and calculations indicate a low activation

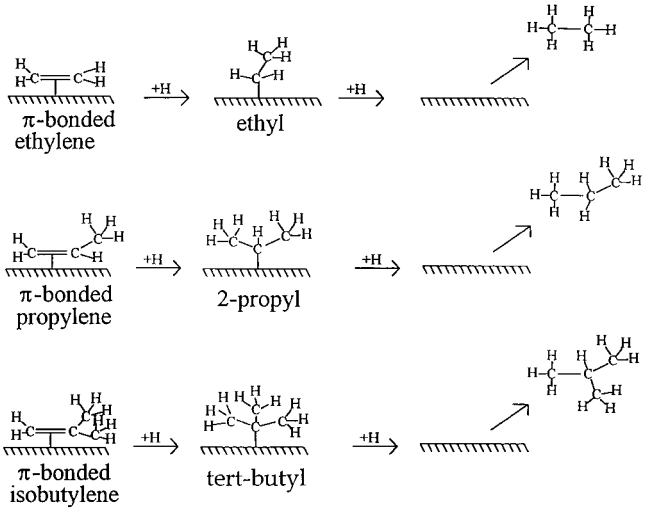

Figure 10. Suggested reaction pathways for ethylene, propylene, and isobutene hydrogenation on Pt(111).

energy for ethylidyne diffusion between the 3-fold sites. After sequential hydrogenation to ethyl and then to ethane the catalytic hydrogenation process repeats.

Propylene[101] and isobutene[102] hydrogenation have also been studied by SFG on Pt(111) at room temperature (Figure 10). Similar to ethylene hydrogenation, propylene and isobutene are hydrogenated stepwise on platinum by atomic hydrogen formed by H_2 dissociation on the surface. The reactions proceed via alkyl intermediates. An issue of interest is the regioselectivity of hydrogen addition to propylene and isobutene, i.e., the position selectivity of hydrogen atom addition to two nonequivalent carbon atoms in the C═C double bond. Hydrogen addition to the terminal carbon yields 2-propyl (isopropyl), while hydrogen addition to the internal carbon forms 1-propyl. Similarly, *tert*-butyl and isobutyl groups result from hydrogen addition to terminal and internal carbons of isobutene. Under reaction conditions of propylene hydrogenation, 2-propyl and π-bonded propylene species were observed on the surface. Vacuum studies indicated that 2-propyl and 1-propyl groups had similar hydrogenation rates. This demonstrates that the 2-propyl group is the reaction intermediate and not just a spectator residing on the surface.

Isobutene hydrogenation has presumably a different reaction mechanism. *tert*-Butyl groups and π-bonded isobutene were the dominant surface species under the reaction conditions, but the hydrogenation rate of *tert*-butyl is much slower than that of isobutyl. As a result, isobutene hydrogenation may be forced to proceed from π-bonded isobutene through the slow kinetic step of isobutyl formation. It provides an explanation of a slow isobutene hydrogenation rate, which is at least 1 order of magnitude lower than those of 1-butene and *cis*-2-butene.[103]

3.4. Cyclohexene Hydrogenation and Dehydrogenation on Pt(111). The dehydrogenation of cyclic alkanes and alkenes to aromatic molecules is one of the key reactions during naphtha reforming.[104] The hydrogenation of olefins is also technologically important. The dehydrogenation and hydrogenation of cyclohexene is a reaction that allows us to obtain information about both processes[105,106] by shifting the equilibrium toward hydrogenation or dehydrogenation by adjusting the hydrogen pressure or the reaction temperature accordingly. Using SFG, we have monitored the molecular species that form upon chemisorption of a monolayer of cyclohexene as a function of temperature and coverage and we have also studied the mechanism of cyclohexene hydrogenation and dehydrogenation over Pt(111) at high pressures and temperatures.

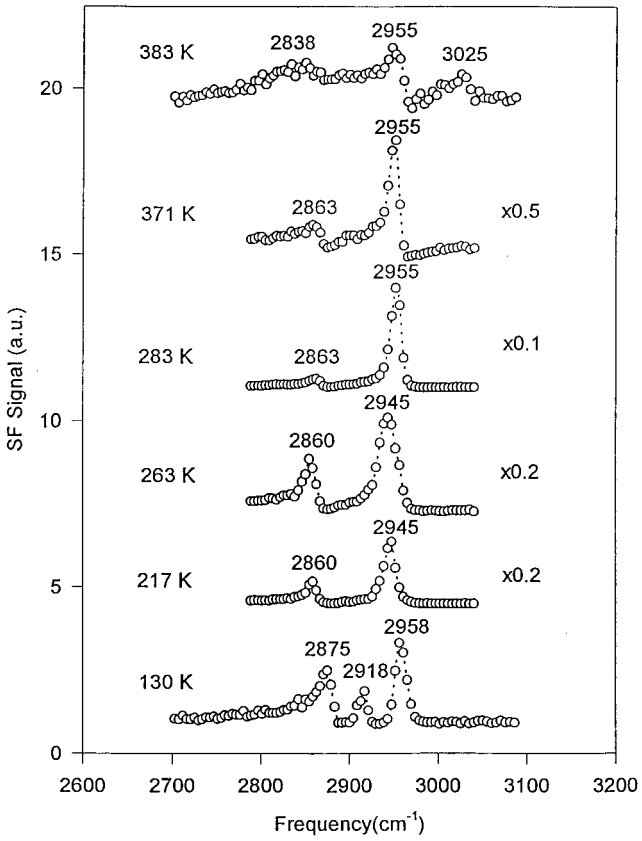

Figure 11. SFG study of cyclohexene on Pt(111) at different surface temperatures.

Previous surface science studies of cyclohexene (C_6H_{10}) chemisorption on Pt(111) in uhv report that the molecule dehydrogenates to benzene readily above 300 K.[105,107−112] Evidence for a c-C_6H_9 intermediate was found from both high-resolution electron energy loss spectroscopy (HREELS) and laser-induced transient desorption Fourier transform mass spectrometry (LITD-FTMS) during the dehydrogenation of cyclohexene (C_6H_{10}) as well as during cyclohexane (C_6H_{12}) dehydrogenation by abstraction of three hydrogen atoms at 220 K.[113,114] Our findings support these results, and we have further explored the mechanism by studying the dehydrogenation of 1,3- and 1,4-cyclohexadienes on Pt(111) in uhv. Both 1,3- and 1,4-cyclohexadiene (C_6H_8) species dehydrogenate to benzene readily around room temperature.[115] Finally, our high-pressure SFG study of cyclohexene dehydrogenation and hydrogenation, the first of its kind, shows 1,4- and 1,3-cyclohexadiene as major surface species.

Cyclohexene Dehydrogenation in uhv. After exposing a clean Pt(111) surface to 4 langmuirs of cyclohexene at 130 K (1 langmuir = 10^{-6} Torr s), the SFG spectrum displayed three features at 2875, 2918, and 2958 cm^{-1} (Figure 11). This spectrum is similar to the Raman spectrum of cyclohexene in the liquid phase[116] (peaks at 2865, 2916, and 2940 cm^{-1}), and based on the assignment there, we ascribe 2875 and 2958 cm^{-1} features to C−H stretch modes in CH_2 groups and the 2918 cm^{-1} peak to the bending mode of the C−H bond.[117] Cyclohexene has a double bond in its molecular structure and has a half-chair conformation with C_2 symmetry in the free molecule.[116,117] A stable half-chair conformation is shown in Figure 12. The double bond is important since cyclohexene donates its π-electron density to the metal as it bonds to the surface. The spectral features observed at 130 K are similar to those of free cyclohexene molecules;[116] therefore, a molecular cyclohexene species is suggested. As a result of the different electronic coupling with the carbon ring, the equatorial C−H appears at a higher stretching frequency than the axial C−H.[118,119] The spectrum is also nearly identical to the Raman spectrum of deuterated cyclohexene 3,3,6,6-d_4 with a small shift in frequencies.[117] In the substituted molecule, the signal comes from CH_2 groups at the C_4 and C_5 positions (Figure 12). Therefore, the SFG features observed at 130 K can then be more specifically assigned to C−H bonds at C_4 and C_5. The lack of seeing any features from CH_2 groups at C_3 and C_6 and CH groups at C_1 and C_2 can be rationalized considering that these C−H bonds are parallel to the surface and the metal surface selection rule prohibits seeing any of the stretching transitions.[120,121] The molecular identity of this species implies that the double bond is barely perturbed or only partially hybridized; therefore, a π/σ hybridized cyclohexene species is suggested. This has also been found by Henn et al.[105] who proposed the formation of a molecular di-σ species.

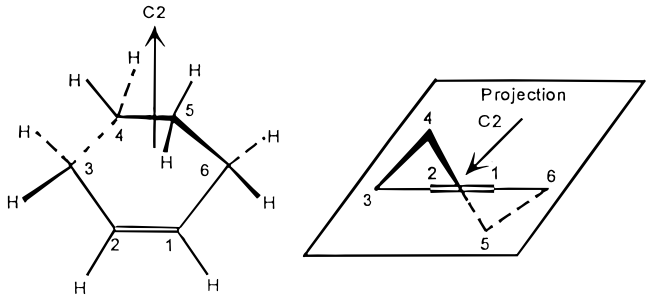

Figure 12. Half-chair conformation of cyclohexene.

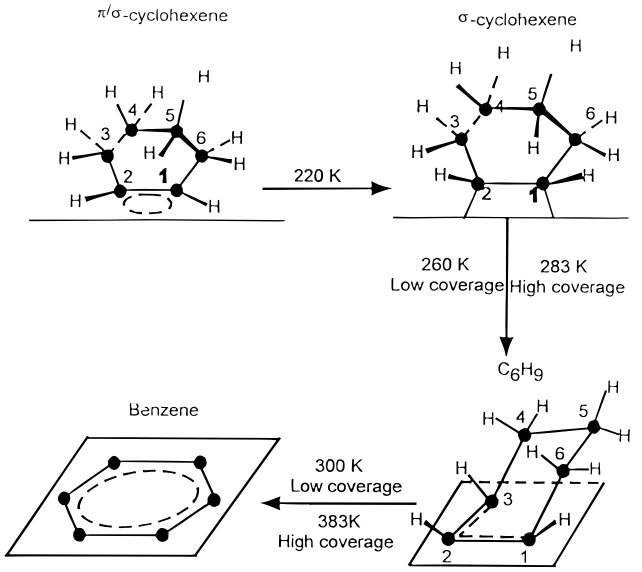

Figure 13. Surface species observed during cyclohexene dehydrogenation on Pt(111).

This molecular species is stable below 200 K, and at 217 K, two new peaks were seen at 2860 and 2945 cm^{-1} and the spectral intensity increased compared to the previous one. The intensity enhancement suggests a more ordered cyclohexene layer on the surface. This result fits very well to a di-σ cyclohexene species (Figure 13), as proposed by others at this temperature.[105] The shift in frequencies of the two features is probably due to the electronic effect as the hybridization of the double bond has changed from sp^2 to sp^3. While the π/σ cyclohexene probably interacts with the metal surface via a side-on geometry (which causes the carbon ring to tilt away from

the surface normal), the carbon ring of the di-σ species will lie closer to the surface normal and hence give a stronger SFG signal.

The spectral features shifted to higher frequency, 2955 and 2863 cm^{-1}, as the surface temperature was raised to 283 K with further enhancement in intensity. Further dehydrogenation occurs, and the observed new species can be assigned to a π-allyl c-C_6H_9 species according to other studies of cyclohexene and cyclohexane decomposition on the same surface.[105,113,114] This assignment is consistent with our spectral results since the stronger peak at 2955 cm^{-1} can be attributed to the equatorial C−H stretching in the c-C_6H_9 species. In this intermediate c-C_6H_9 (shown in Figure 13), the equatorial C−H on the C_6 position carbon is nearly vertical since half the carbon ring is nearly perpendicular to the surface. This shows the stepwise tilting of the carbon ring toward the metal surface as it dehydrogenates to the final product benzene.

This species survived on the surface until 371 K and further decomposition and dehydrogenation occurred above this temperature as evidenced by the greatly attenuated spectral intensity and the appearance of the 3025 cm^{-1} peak, which implies the presence of sp^2 carbon species (Figure 11). The observed temperature of benzene formation is higher than that reported by others.[105] This is probably due to a higher coverage of cyclohexene on the surface in our study. The upshift of the dehydrogenation temperature is apparently due to a site-blocking effect which has also been observed in other hydrocarbon molecule decompositions on Pt(111).[122] Since the sites needed for dehydrogenation of the C_6H_9 species are not readily available at high coverage, this affects the chemistry in the decomposition pathway. Only at higher temperature do the species desorb or decompose and make available the necessary dehydrogenation sites. On the basis of the above discussion, a reaction pathway as shown in Figure 13 is proposed.

SFG Spectra of 1,3- and 1,4-Cyclohexadiene on Pt(111) in uhv. An SFG spectrum recorded after exposing Pt(111) at 130 K to 1 langmuir 1,3-CHD is shown in Figure 14a. Four peaks at 2830, 2875, 2900, and 3020 cm^{-1} and a shoulder at 2770 cm^{-1} appear in the spectrum. The 2830, 2875, and 2900 cm^{-1} features can be assigned to the C−H stretch modes of CH_2 and the 3020 cm^{-1} peak to the CH stretch mode of the C═C−H group of 1,3-CHD on the surface, since they correspond well with those in the infrared spectrum of the same molecule in the gas phase.[123,124] An infrared spectrum of 1,3-CHD in the liquid phase is also shown for comparison (Figure 14b). The close coincidence in frequencies between the SFG features and the infrared peaks indicates that 1,3-CHD adsorbs intact on the surface. The nonplanar conformation of the 1,3-CHD molecule with two CH_2 groups pointing in opposite directions hinders the interaction between its π-electrons and the d-orbitals of surface Pt metal atoms and could probably result in a tilted configuration of the adsorbed 1,3-CHD molecule on the surface. This geometry has a significant consequence on the chemistry of 1,3-CHD upon annealing.

Figure 15a represents an SFG vibrational spectrum recorded after 1 langmuir exposure of 1,4-CHD on Pt(111) at 130 K. Only a sharp peak at 2770 cm^{-1} with a peak width of ~12 cm^{-1} at the half-maximum was observed. 1,4-CHD in the gas phase has a nearly planar configuration with its π-orbitals perpendicular to the molecular plane. Therefore, the molecule should adsorb flat on the surface to facilitate the interaction between its π-electrons and the d-orbitals of the surface Pt atoms. It has been shown by Hugenschmidt et al.[125] that 1,4-CHD adsorbs molecularly on the surface below 230 K, but our

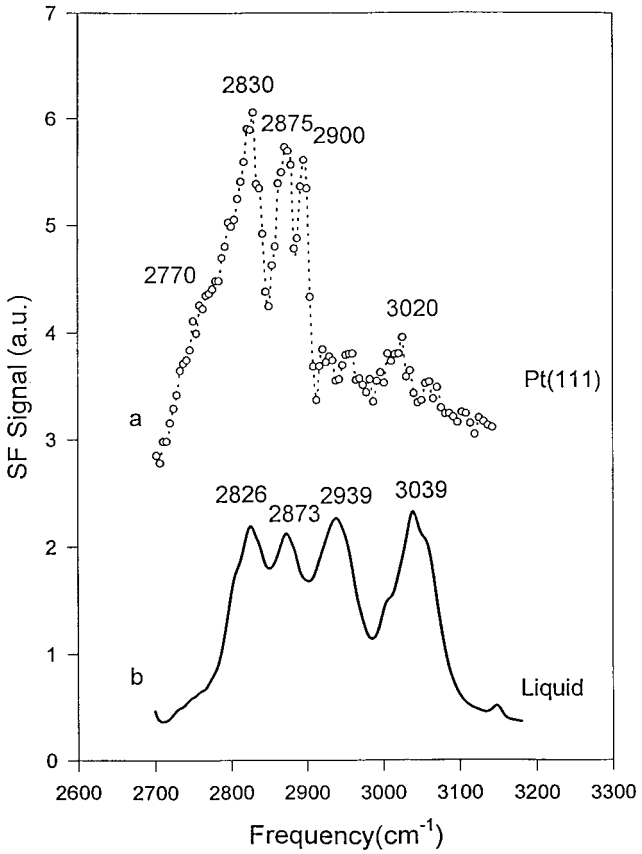

Figure 14. (a) Typical SFG spectrum of a monolayer of 1,3-cyclohexadiene on Pt(111) at 130 K. (b) Infrared spectrum in the liquid phase.

spectrum is very different from the infrared spectrum of the liquid 1,4-CHD (Figure 15b). This spectral result can be explained by a flat, "quatra-σ-bonding" adsorption geometry.[125] The C−H bonds in the C═C−H group are in the molecular plane and parallel to the surface and thus give no SFG signal due to the selection rule on metal surfaces.[120,121] The feature observed in the spectrum is then assigned to the C−H stretch mode in the CH_2 groups. The axis of the CH_2 groups points along the metal surface, therefore, only the asymmetric CH stretch mode has a nonzero dipole moment along the surface normal and contributes to the signal. The frequency of the 2770 cm^{-1} peak is about 50−100 cm^{-1} red-shifted from the C−H stretch modes found for 1,4-CHD in the gas phase (i.e., symmetric stretch 2825 cm^{-1} and antisymmetric stretch 2875 cm^{-1}, respectively).[123,124] The red-shift indicates C−H bond weakening. This is probably due to the strong electron-withdrawing effect from the surface Pt atoms, and consequently, the electron density in the two C−H bonds flows to the surface Pt atoms and weakens the bond between C and H.

The temperature dependence of the SFG spectra of 1,4-CHD on Pt(111) is presented in Figure 16. 1,4-Cyclohexadiene does not dehydrogenate significantly up to 283 K, as one can conclude from the spectra. Above 300 K, the signal from adsorbed 1,4-CHD disappeared completely. This is due to the dehydrogenation of 1,4-CHD to benzene at this temperature, as revealed by bismuth postdosing thermal desorption mass spectroscopy (BPTDS) studies on the same system.[125] The weak feature at 3030 cm^{-1} is probably from the adsorbed benzene fragments. The dehydrogenation happens via a hydrogen abstraction mechanism instead of β-hydrogen elimination from the CH_2 group, as indicated by activation energy measurements.[125,126]

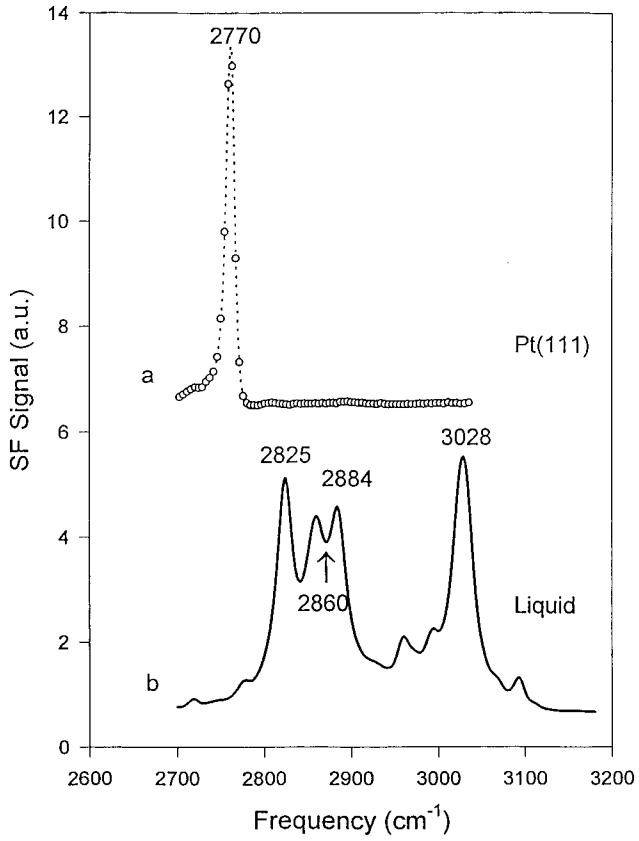

Figure 15. (a) Typical SFG spectrum for a monolayer of 1,4-cyclohexadiene on Pt(111) at 130 K. (b) Infrared spectrum in the liquid phase.

The temperature dependence of the SFG spectra of adsorbed 1,3-CHD is more complex (Figure 17). With increasing temperature, the 2770 cm^{-1} feature grows while those characteristic of the adsorbed 1,3-CHD decrease. At 283 K, the 2770 cm^{-1} peak becomes the major feature in the spectrum, but it disappears above 300 K, leaving a weak feature at 3030 cm^{-1} that indicates the presence of benzene as the final product in the thermal evolution.[112,125] The 2770 cm^{-1} peak is identical to that for the adsorbed 1,4-CHD in Figure 16. This is a clear evidence that 1,4-CHD is present on the Pt surface before 1,3-CHD completely dehydrogenates to benzene. 1,4-CHD formation can occur either through a rearrangement of the hydrogen atoms in 1,3-CHD molecules or by a dehydrogenation−hydrogenation process. However, we did not observe any 1,4-CHD formation on this surface in benzene−hydrogen coadsorption experiments, and this excludes the possibility of the existence of the dehydrogenation−hydrogenation process. The slight increase in intensity of the weak features at high frequency during 1,3-CHD thermal evolution implies that dehydrogenation to benzene is also a possible reaction pathway. Therefore, upon annealing dehydrogenation and isomerization surface reactions are in competition. A scheme of the two reaction branches is shown below.

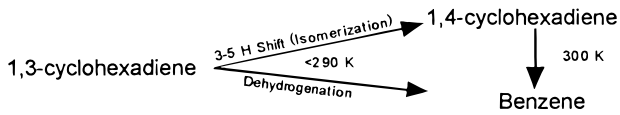

Cyclohexene Hydrogenation and Dehydrogenation at High Pressures. High-pressure reaction studies were carried out typically at 10 Torr cyclohexene with various hydrogen pressures (20−590 Torr) and in the temperature range of 295−560 K. Under these conditions, the prominent feature in the surface SFG spectrum at 295 K is at 2765 cm^{-1} (Figure 18). This feature was attributed to 1,4-CHD on the surface. The smaller peaks in the spectrum were from 1,3-CHD. The assignment of the spectrum was made by comparison to the CHD spectra in uhv (Figures 14−17). Interestingly, there was no evidence for cyclohexene C_6H_{10} and c-C_6H_9 species on the surface, which are the important species in cyclohexene dehydrogenation in uhv (Figures 11 and 13).

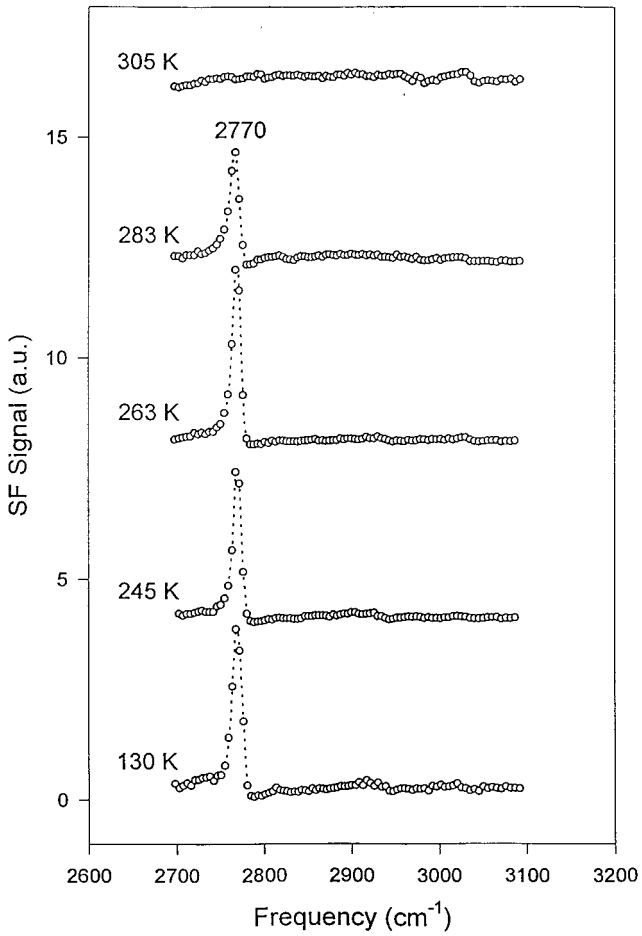

Figure 16. Temperature dependence of the SFG spectrum of 1,4-cyclohexadiene on Pt(111) under ultrahigh vacuum.

Above 300 K, the 2765 cm^{-1} peak disappeared and the weak 1,3-CHD features in the spectrum at 295 K became stronger and dominated the spectrum. The vibrational SFG spectrum remains unchanged in the temperature range 300−400 K (spectrum at 403 K in Figure 18). Further increasing the surface temperature to 480 K, the feature representing 1,4-CHD appeared in the spectrum again in addition to the features from 1,3-CHD. This spectrum indicates that both 1,3-CHD and 1,4-CHD coexist on the surface during a high-pressure reaction.

The reaction kinetics were also measured as a function of both temperature and hydrogen pressure. The hydrogenation rate was greatly enhanced with increasing surface temperature and reached its maximum rate of 77 molecules/site/second around 400 K at 10 Torr cyclohexene/100 Torr H_2 (Figure 19). Above 400 K, dehydrogenation became observable and suppressed the hydrogenation reaction. The maximum dehydrogenation rate of 58 molecules/site/second was obtained at 480 K (Figure 19).

The reaction is almost first order in hydrogen pressure below 200 Torr, and the order dependence declines as the pressure is increased. This implies that a saturation of hydrogen on the surface is approached at high hydrogen pressure. It should be

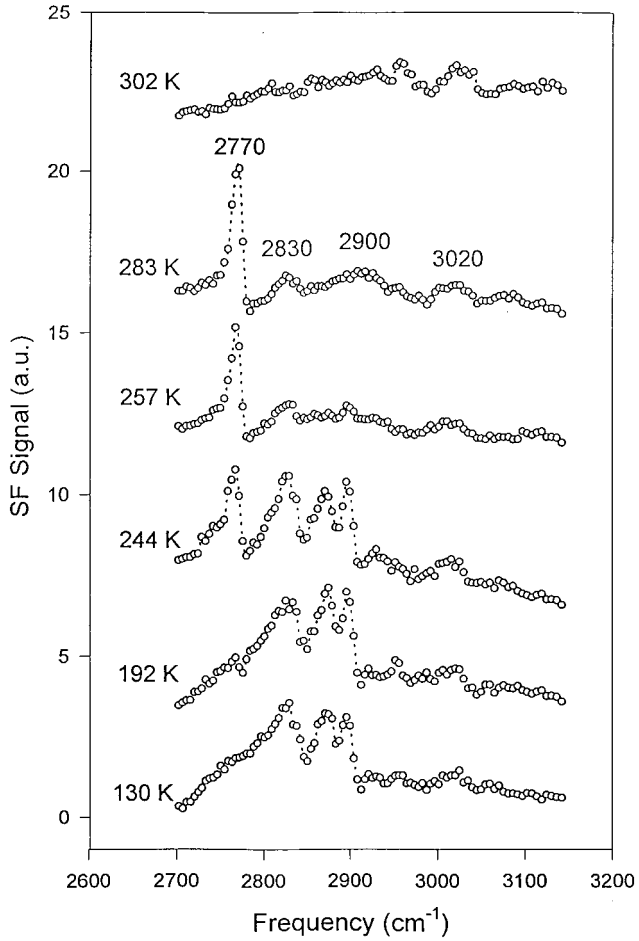

Figure 17. SFG spectra for 1,3-cyclohexadiene on Pt(111) at different crystal temperatures.

noted that, at 403 K, the dehydrogenation almost exhibits zero-order dependence on hydrogen pressure. This is probably due to the low probability of desorption of benzene that slows down dehydrogenation at this temperature.[112]

Since the dehydrogenation reaction rate is zero as revealed by gas composition analysis in the temperature range 300−400 K (Figure 19), we can make the approximation that only hydrogenation occurs in this temperature range. Thus, the Arrhenius law can be applied to the hydrogenation reaction and an activation energy of 37 kJ/mol for the hydrogenation reaction at a reaction condition of 10 Torr cyclohexene and 100 Torr of hydrogen was obtained. This is in agreement with results from Segal et al. who obtained an activation energy of ∼33 kJ/mol for this reaction in studies over supported platinum catalysts.[127] The measured hydrogenation rate drops quickly above 400 K, while the dehydrogenation rate increased rapidly (Figure 19).

The Arrhenius behavior of the hydrogenation in this range (300−400 K) implies that the number of surface-active sites for hydrogenation does not change in any significant manner in the temperature range 300−400 K. The absence of 1,4-CHD in the spectrum indicates that the surface concentration of this species is very low. This allows us to conclude that 1,3-CHD is the likely surface reaction intermediate during cyclohexene hydrogenation. It has been found that at room temperature 1,4-CHD on the surface inhibits reactions as a full monolayer coverage is reached[112] and this excludes the possibility that 1,4-CHD is an intermediate for hydrogenation in this temperature range.

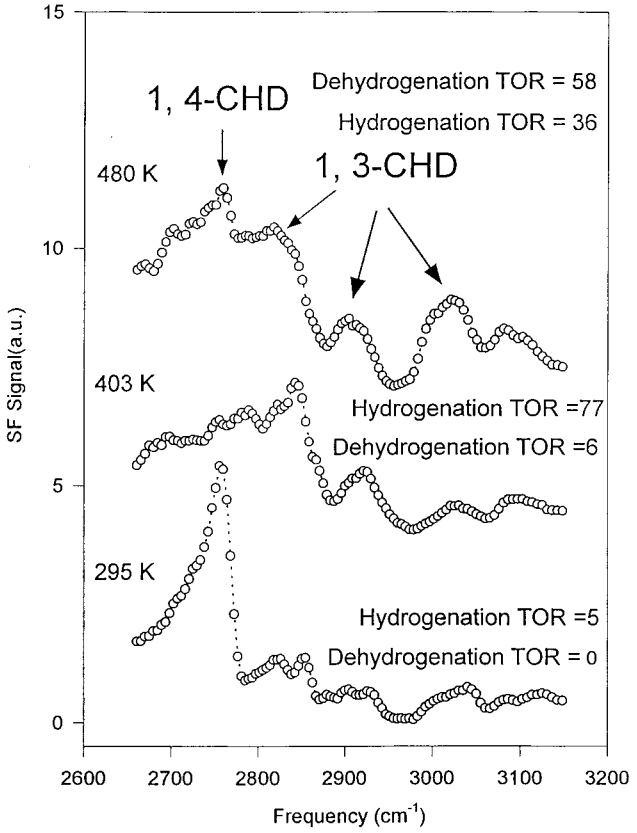

Figure 18. Temperature dependence of the SFG spectrum during high-pressure cyclohexene conversion on Pt(111) at 10 Torr cyclohexene/100 Torr hydrogen (TOR is the abbreviation of turnover rate).

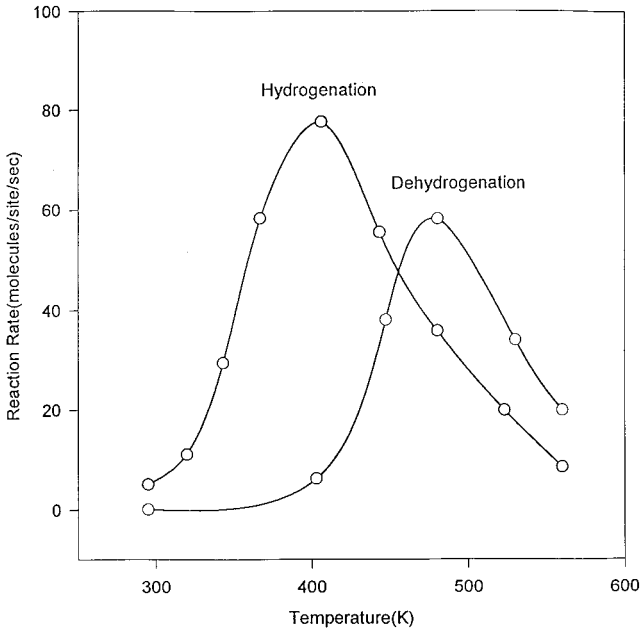

Figure 19. Temperature dependence of hydrogenation and dehydrogenation reactions on Pt(111) at 10 Torr cyclohexene/100 Torr hydrogen.

To confirm the above conclusion, we carried out the hydrogenation of both 1,3- and 1,4-CHD at 295 K as shown in parts a and b of Figure 20. As expected, 1,3-CHD hydrogenates very fast with a rate of ∼100 molecules/site/second, while a much lower rate of only ∼5 molecules/site/second was obtained for 1,4-CHD at 295 K. This correlation between the adsorbed surface species and their hydrogenation kinetics supports the

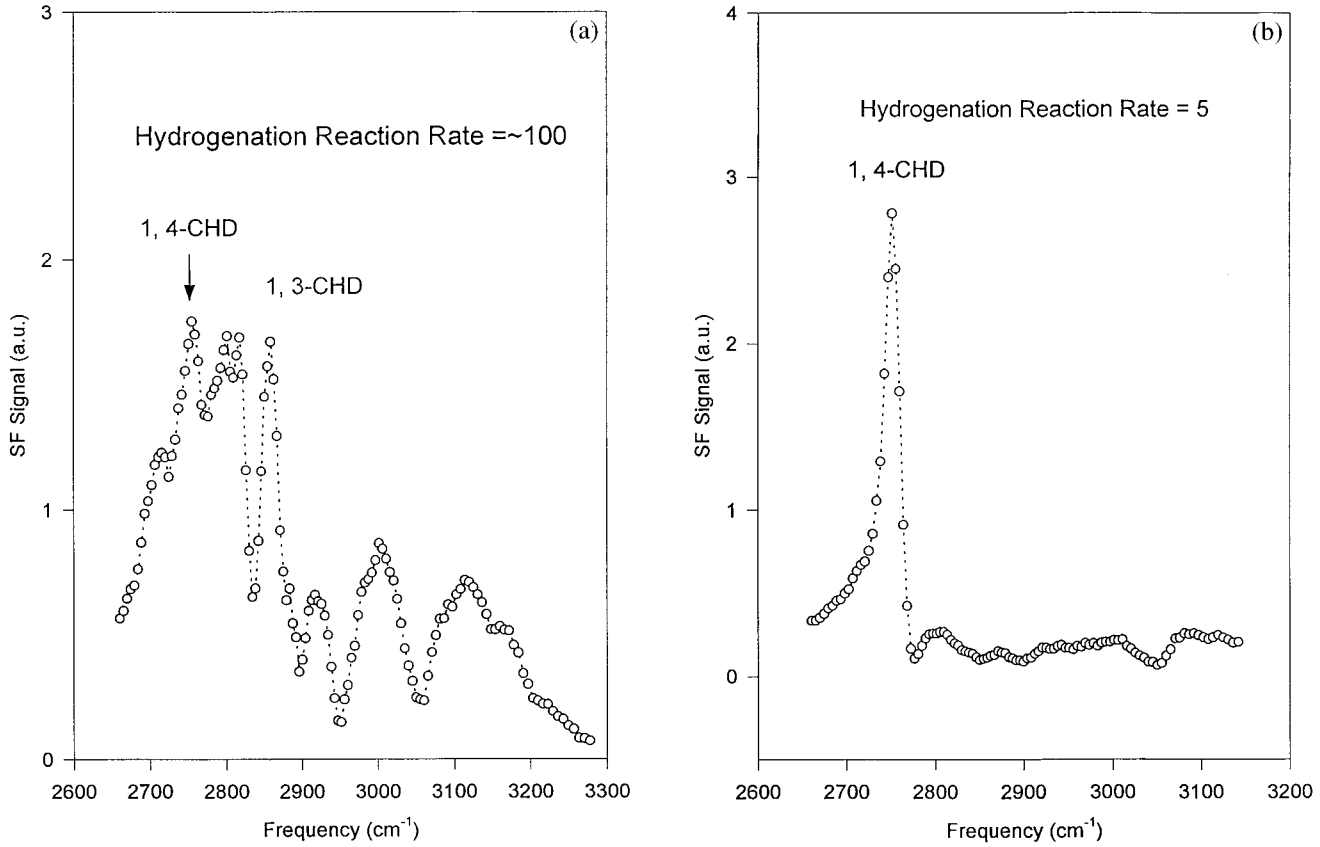

Figure 20. In situ SFG spectrum of high-pressure hydrogenation of (a) 1,3-cyclohexadiene and (b) 1,4-cyclohexadiene over Pt(111) (TOR is the abbreviation of turnover rate).

above conclusion that 1,3-CHD is the intermediate in cyclohexene hydrogenation.

Above 400 K, the platinum surface carries out both hydrogenation and dehydrogenation. The dehydrogenation rate reached its peak at 480 K. This shift must be related to the active surface sites that change from performing hydrogenation to carrying out dehydrogenation. The steep drop of the hydrogenation rate can also partly be attributed to the fact that 1,3-CHD is unstable at high temperature and it either dehydrogenates to benzene or rearranges to its 1,4-isomer and contributes directly or indirectly to the dehydrogenation reaction path.

Both hydrogenation and dehydrogenation reaction rates decrease as the temperature is raised above 500 K (Figure 19). This could be due to the deactivation of the surface as carbonaceous species accumulate. It is also possible that the adsorption rate of cyclohexene limited the reactions. A reaction mechanism can be suggested as follows:

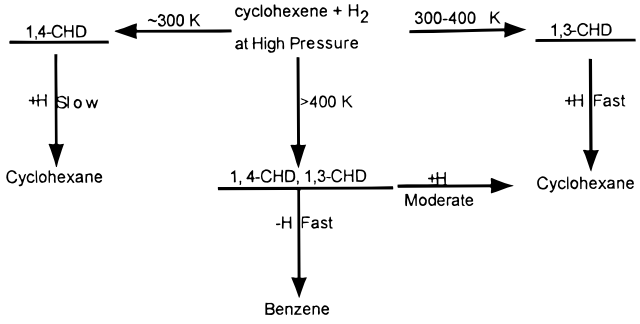

4. Summary and Future Directions

IR−visible sum frequency generation has proven to be a very powerful in situ method to obtain surface-specific chemical information at both high and low pressures (i.e., uhv and atmospheres of gases). The ability to monitor the structure and concentration of active intermediates on the surface with chemical specificity during realistic reaction conditions should greatly contribute toward understanding the molecular processes. It will be invaluable to exploit SFG vibrational spectroscopy to explore the nature of the surface chemical bonds and the concentration of intermediate species for a wide range of catalytic reactions.

During our studies of adsorption and catalytic reactions on single-crystal surfaces, we have found a number of surprising results. Corrosive chemisorption of CO on Pt and Rh(111) as observed by SFG is an extreme case of chemisorption-induced restructuring of metal surfaces. Metal atoms break away from step or kink surface sites and form bonds with several adsorbate molecules. Carbon monoxide can form several carbonyl ligand bonds with platinum atoms leading to the creation of metal−carbonyl species. Thus, metal−metal bonds are broken in favor of forming metal−carbonyl clusters that are more stable at high CO pressures. The SFG vibrational spectra detect the reversible formation of new adsorbed carbon monoxide species above 100 Torr on Pt(111) that appear to be platinum−carbonyl clusters $Pt_n(CO)_m$, with $(m/n) > 1$ and a CO incommensurate overlayer. Furthermore, SFG revealed new CO species in CO oxidation and provided strong evidence for their active role for oxidation to CO_2.

During ethylene hydrogenation over Pt(111), the reaction intermediate which produces most of the ethane appears to be weakly bound π-bonded ethylene (which appears only at higher reactant pressures after all the strongly adsorbing sites on the metal surface are occupied), while ethylidyne and di-σ-bonded ethylene are spectators during the catalytic process. The surface concentration of π-bonded ethylene is 4% of a monolayer during

the reaction, which yields an absolute turnover rate 25 times higher than the turnover rate per platinum atom.

Cyclohexene dehydrogenates to benzene through π/σ, di-σ and c-C_6H_9 species under uhv on Pt(111) upon heating. A site-blocking effect was observed at saturation coverage of cyclohexene which caused the dehydrogenation to shift to higher surface temperature. The structure and reactions of 1,3-cyclohexadiene and 1,4-cyclohexadiene have also been studied in uhv. 1,4-CHD adsorbs flat on the surface and dehydrogenates to adsorbed benzene at about 300 K. 1,3-CHD undergoes a rearrangement to 1,4-CHD through a 3−5 hydrogen shift, which competes with the dehydrogenation reaction pathway at low temperature (<290 K). During the high-pressure hydrogenation of cyclohexene unexpected surface species were observed. 1,4- and 1,3-cyclohexadiene were the major surface species under all experimental conditions explored in this study, even in the presence of 600 Torr of hydrogen. 1,3-CHD was found to be the dominant surface species during the hydrogenation reaction in the temperature range of 300−400 K and appears to be the reaction intermediate. Above 400 K, the surface carries out both hydrogenation and dehydrogenation reactions and both 1,3- and 1,4-CHD coexist on the Pt(111) surface as found by SFG spectroscopy. This indicates that both CHDs are precursors for benzene formation. Monitoring the reaction kinetics and the chemical nature of surface species in parallel allowed us to postulate a reaction mechanism where cyclohexene hydrogenates to cyclohexane preferentially via a 1,3-CHD intermediate and dehydrogenates to benzene through both 1,4-CHD and 1,3-CHD intermediates.

Perhaps the most striking result is the detection of *dehydrogenated* reaction intermediates during *hydrogenation* reactions (e.g., ethylidyne, 1,4-CHD, and 1,3-CHD) and the presence of stagnant, spectator species. The active species may only appear at high pressure, illustrating the need to cover a wide pressure range during vibrational studies. All our studies of chemisorption and catalytic reactions at high pressures indicate that the metal surface is dynamic; it changes its surface structure as the chemisorbing atoms or molecules have changed. There is mobility of metal atoms on the metal surface, of adsorbates in the adsorbed overlayer, and the surface defects may also restructure.

In the future, SFG will presumably be further improved by the expansion of the frequency range below 1100 cm^{-1} and by the development of methods to apply SFG to microporous surfaces. An increased time resolution will allow us to monitor dynamic processes such as the motion of surface atoms and molecules, their diffusion, rotation, vibrational and electronic excitation, and their reaction dynamics. By measuring the surface coverage as a function of reactant pressure and temperature and monitoring the structure of the adsorbed species in parallel, *molecular adsorption isotherms* can be obtained. The application of the technique to catalytic reactions at solid−liquid interfaces[128] will result in rapid developments benefiting catalysis, electrochemistry (electrocatalysis), and biology.[74,129]

Acknowledgment. This work was supported by the Director, Office of Energy Research, Office of Basic Energy Sciences, Materials Sciences Division of the U.S. Department of Energy under Contract DE-AC03-76SF00098.

References and Notes

(1) Somorjai, G. A. *Introduction to Surface Chemistry and Catalysis*; John Wiley & Sons: New York, 1994.
(2) Somorjai, G. A. *Surf. Sci.* **1994**, *299/300*, 849.
(3) Goodman, D. W. *Chem. Rev.* **1995**, *95*, 523.
(4) Ertl, G. *Surf. Sci.* **1994**, *299/300*, 742.
(5) Woodruff, D. P.; Delchar, T. A. *Modern Techniques of Surface Science*; Cambridge University Press: New York, 1986.
(6) Somorjai, G. A.; Rupprechter, G. *J. Chem. Educ.* **1998**, *75*, 161.
(7) Blakely, D. W.; Kozak, E.; Sexton, B. A.; Somorjai, G. A. *J. Vac. Sci. Technol.* **1976**, *13*, 1091.
(8) Cabrera, A. L.; Spencer, N. D.; Kozak, E.; Davies, P. W.; Somorjai, G. A. *Rev. Sci. Instrum.* **1982**, *53*, 1888.
(9) Rupprechter, G.; Somorjai, G. A. *Catal. Lett.* **1997**, *48*, 17.
(10) Davis, S. M.; Zaera, F.; Somorjai, G. A. *J. Am. Chem. Soc.* **1982**, *104*, 7453.
(11) Ribeiro, F. H.; Gerken, C. A.; Rupprechter, G.; Somorjai, G. A.; Kellner, C. S.; Coulston, G. W.; Manzer, L. E.; Abrams, L. *J. Catal.* **1998**, *176*, 352.
(12) Starke, U.; Hove, M. A. V.; Somorjai, G. A. *Prog. Surf. Sci.* **1994**, *46*, 305.
(13) Gauthier, Y.; Baudoing-Savois, R.; Heinz, K.; Landskron, H. *Surf. Sci.* **1991**, *251*, 493.
(14) Shih, H. E.; Jona, F.; Marcus, P. M. *Phys. Rev. Lett.* **1981**, *46*, 731.
(15) Wander, A.; Van Hove, M. A.; Somorjai, G. A. *Phys. Rev. Lett.* **1991**, *67*, 626.
(16) Somorjai, G. A. *Langmuir* **1991**, *7*, 3176.
(17) Somorjai, G. A. *Chem. Rev.* **1996**, *96*, 1223.
(18) Shen, Y. R. *Surf. Sci.* **1994**, *299/300*, 551.
(19) Du, Q.; Superfin, R.; Freysz, E.; Shen, Y. R. *Phys. Rev. Lett.* **1993**, *70*, 2313.
(20) Johal, M. S.; Ward, R. N.; Davies, P. B. *J. Phys. Chem.* **1996**, *100*, 274.
(21) Conboy, J. C.; Messmer, M. C.; Richmond, G. L. *J. Phys. Chem.* **1996**, *100*, 7617.
(22) Shen, Y. R. *Nature* **1989**, *337*, 519.
(23) Shen, Y. R. *The Principles of Nonlinear Optics*; John Wiley Inc.: New York, 1984.
(24) Cremer, P. S.; McIntyre, B. J.; Salmeron, M.; Shen, Y. R.; Somorjai, G. A. *Catal. Lett.* **1995**, *34*, 11.
(25) Cremer, P. S.; Somorjai, G. A. *J. Chem. Soc., Faraday Trans.* **1995**, *91*, 3671.
(26) Cremer, P. S.; Stanners, C.; Niemantsverdriet, J. W.; Shen, Y. R.; Somorjai, G. A. *Surf. Sci.* **1995**, *328*, 111.
(27) Cremer, P. S.; Su, X.; Shen, Y. R.; Somorjai, G. A. *J. Am. Chem. Soc.* **1996**, *118*, 2942.
(28) Somorjai, G. A.; Rupprechter, G. In *Dynamics of Surfaces and Reaction Kinetics in Heterogeneous Catalysis*; Studies in Surface Science and Catalysis Series 109; Froment, G. F., Waugh, K. C., Eds.; Elsevier: Amsterdam, 1997; p 35.
(29) Carpick, R.; Salmeron, M. *Chem. Rev.* **1997**, *97*, 1163.
(30) Lio, A.; Reichert, A.; Nagy, J. O.; Salmeron, M. *J. Vac. Sci. Technol.* **1996**, *14*, 1481.
(31) Spiewak, B. E.; Cortright, R. D.; Dumesic, J. A. *J. Catal.* **1998**, *176*, 405.
(32) Shen, J.; Spiewak, B. E.; Dumesic, J. A. *Langmuir* **1997**, *13*, 2735.
(33) Baker, R. T. K. *J. Adhes.* **1995**, *52*, 13.
(34) Rodriguez, N. M.; Oh, S. G.; Dallabetta, R. A.; Baker, R. T. K. *J. Catal.* **1995**, *157*.
(35) Matyshak, V. A.; Il′ichev, A. N.; Ukharsky, A. A.; Korchak, V. N. *J. Catal.* **1997**, *171*, 245.
(36) Schlienz, H.; Beckendorf, M.; Katter, U. J.; Risse, T.; Freund, H.-J. *Phys. Rev. Lett.* **1995**, *74*, 761.
(37) Meitzner, G. D.; Iglesia, E.; Baumgartner, J. E.; Huang, E. S. *J. Catal.* **1993**, *140*, 209.
(38) Fisher, I. A.; Bell, A. T. *J. Catal.* **1997**, *172*, 222.
(39) Suer, M. G.; Dardas, Z.; Ma, Y.; Moser, W. R. *J. Catal.* **1996**, *162*, 320.
(40) Dardas, Z.; Suer, M. G.; Ma, Y.; Moser, W. R. *J. Catal.* **1996**, *159*, 204.
(41) Zaera, F.; Janssens, T. V. W.; Ofner, H. *Surf. Sci.* **1996**, *368*, 371.
(42) Arumainayagam, C. R.; Tripa, C. E.; Xu, J. Z.; Yates, J. T. *Surf. Sci.* **1996**, *360*, 121.
(43) Fan, J. F.; Yates, J. T. *J. Am. Chem. Soc.* **1996**, *118*, 4686.
(44) Janssens, T. V. W.; Jin, G. L.; Zaera, F. *J. Am. Chem. Soc.* **1997**, *119*, 1169.
(45) Bodker, F.; Morup, S.; Oxborrow, C. A.; Linderoth, S. *J. Phys. Condens. Matter* **1992**, *31*, 6555.
(46) Bodker, F.; Morup, S.; Niemantsverdriet, J. W. *Catal. Lett.* **1992**, *13*, 195.
(47) Haw, J. F.; Goguen, P. W.; Xu, T.; Skloss, T. W. *Angew. Chem., Int. Ed. Engl.* **1998**, *37*, 948.
(48) Goguen, P. W.; Haw, J. F. *J. Catal.* **1996**, *161*, 870.
(49) Ferguson, D. B.; Haw, J. F. *Anal. Chem.* **1995**, *67*, 3342.
(50) Anderson, B. G.; vanSanten, R. A.; Ijzendoorn, L. J. *Appl. Catal. A* **1997**, *160*, 125.

(51) Jonkers, G.; Vonkeman, K. A.; Vanderwal, S. W. A.; van Santen, R. A. *Nature* **1992**, *355*, 63.
(52) Weckhuysen, B. M.; Wachs, I. E. *J. Phys. Chem. B* **1997**, *101*, 2793.
(53) Wachs, I. E.; Jehng, J. M.; Deo, G.; Weckhuysen, B. M. *Catal. Today* **1996**, *32*, 47.
(54) Xie, S. B.; Mestl, G.; Rosynek, M. P.; Lunsford, J. H. *J. Am. Chem. Soc.* **1997**, *119*, 10186.
(55) Jensen, J. A.; Rider, K. B.; Salmeron, M.; Somorjai, G. A. *Phys. Rev. Lett.* **1998**, *80*, 1228.
(56) Somorjai, G. A. *MRS Bull.* **1998**, *23*, 11.
(57) Su, X.; Jensen, J.; Yang, M. X.; Salmeron, M. B.; Shen, Y. R.; Somorjai, G. A. *Faraday Discuss.* **1996**, *105*, 263.
(58) Zou, S. Z.; Weaver, M. J. *Anal. Chem.* **1998**, *70*, 2387.
(59) Zou, S. Z.; Williams, C. T.; Chen, E. K. Y.; Weaver, M. J. *J. Am. Chem. Soc.* **1998**, *120*, 3811.
(60) Tolia, A. A.; Smiley, R. J.; Delgass, W. N.; Takoudis, C. G. *J. Catal.* **1994**, *150*, 56.
(61) Stair, P. C.; Li, C. *J. Vac. Sci. Technol.* **1997**, *15*, 1679.
(62) Li, C.; Stair, P. C. *Catal. Lett.* **1996**, *36*, 119.
(63) Clausen, B. S.; Steffensen, G.; Fabius, B.; Villadsen, J. *J. Catal.* **1991**, *132*, 524.
(64) Clausen, B. S.; Topsoe, H. *Catal. Today* **1991**, *9*, 189.
(65) Mukerjee, S.; Thurston, T. R.; Jisrawi, N. M.; Yang, X. Q. *J. Electrochem. Soc.* **1998**, *145*, 466.
(66) Guyot-Sionnest, P.; Hunt, J. H.; Shen, Y. R. *Phys. Rev. Lett.* **1987**, *59*, 1597.
(67) Busca, G. *Catal. Today* **1996**, *27*, 323.
(68) Wang, H.; Borguet, E.; Yan, E. C. D.; Zhang, D.; Gutow, J.; Eisenthal, K. B. *Langmuir* **1998**, *14*, 1472.
(69) Maytorena, J. A.; Mendoza, B. S.; Mochan, W. L. *Phys. Rev. B* **1998**, *57*, 2569.
(70) Domen, K.; Hirose, C. *Appl. Catal. A* **1997**, *160*, 153.
(71) Richmond, G. L. *Anal. Chem.* **1997**, *69*, 536.
(72) Kato, T.; Hayashi, M.; Villaeys, A. A.; Lin, S. H. *Phys. Rev. A* **1997**, *56*, 980.
(73) Hirose, C.; Yamamoto, H.; Akamatsu, N.; Domen, K. *J. Chem. Phys.* **1993**, *97*, 10064.
(74) Zhang, D.; Shen, Y. R.; Somorjai, G. A. *Chem. Phys. Lett.* **1997**, *281*, 394.
(75) Härle, H.; Lehnert, A.; Metka, U.; Volpp, H. R.; Willms, L.; Wolfrum, J. *Chem. Phys. Lett.* **1998**, *293*, 26.
(76) Zhang, J.; Huang, J.; Shen, Y. R.; Chen, C. *J. Opt. Soc. Am.* **1993**, *10*, 1758.
(77) Zhu, X. D.; Suhr, H.; Shen, Y. R. *Phys. Rev. B* **1987**, *35*, 3047.
(78) Rupprechter, G.; Kung, K.; Somorjai, G. A. In preparation.
(79) Steininger, H.; Lehwald, S.; Ibach, H. *Surf. Sci.* **1982**, *117*, 342.
(80) Avery, N. R. *J. Chem. Phys.* **1981**, *74*, 4202.
(81) Hayden, B. E.; Bradshaw, A. M. *Surf. Sci.* **1983**, *125*, 787.
(82) Superfine, R.; Huang, J. Y.; Shen, Y. R. *Opt. Lett.* **1987**, *15*, 1276.
(83) Crossley, A.; King, D. A. *Surf. Sci.* **1977**, *68*, 528.
(84) Su, X.; Cremer, P. S.; Shen, Y. R.; Somorjai, G. A. *Phys. Rev. Lett.* **1996**, *77*, 3858.
(85) Warnaby, C. E.; Stuch, A.; Yeo, Y. Y.; King, D. A. *J. Chem. Phys.* **1995**, *102*, 22.
(86) Huber, H.; Kündig, E. P.; Moxkovits, M.; Ozin, G. A. *J. Am. Chem. Soc.* **1973**, *95*, 332.
(87) Wander, A.; Hove, M. A. V.; Somorjai, G. A. *Phys. Rev. Lett.* **1991**, *67*, 626.
(88) Kung, K.; Su, X.; Rupprechter, G.; Somorjai, G. A. In preparation.
(89) Anderson, J. A. *J. Chem. Soc., Faraday Trans.* **1992**, *88*, 1197.
(90) Campbell, C. T.; Ertl, G.; Kuipers, H.; Segner, J. *J. Chem. Phys.* **1980**, *73*, 5862.
(91) Horiuti, I.; Polanyi, M. *Trans. Faraday Soc.* **1934**, *30*, 1164.
(92) Mohsin, S.; Trenary, M.; Robota, H. *J. Phys. Chem.* **1988**, *92*, 5229.
(93) Rekoske, J. E.; Cortright, R. D.; Goddard, S. A.; Sharma, S. B.; Dumesic, J. A. *J. Phys. Chem.* **1992**, *96*, 1880.
(94) Beebe, T.; Yates, J. T. *J. Am. Chem. Soc.* **1986**, *108*, 663.
(95) Davis, S. M.; Zaera, F.; Gordon, B. E.; Somorjai, G. A. *J. Catal.* **1985**, *92*, 250.
(96) Steiniger, H.; Ibach, H.; Lehwald, S. *Surf. Sci.* **1992**, *117*, 685.
(97) Cremer, P. S.; Su, X.; Shen, Y. R.; Somorjai, G. A. *Catl. Lett.* **1996**, *40*, 143.
(98) Schlatter, J.; Boudart, M. *J. Catal.* **1972**, *24*, 482.
(99) Cortright, R.; Goddard, S.; Rekoske, J.; Dumesic, J. *J. Catal.* **1991**, *127*, 342.
(100) Döll, R.; Gerken, C. A.; Hove, M. A. V.; Somorjai, G. A. *Surf. Sci.* **1997**, *374*, 151.
(101) Cremer, P. S.; Su, X.; Shen, Y. R.; Somorjai, G. A. *J. Phys. Chem.* **1996**, *100*, 16302.
(102) Cremer, P. S.; Su, X.; Shen, Y. R.; Somorjai, G. A. *J. Chem. Soc., Faraday Trans.* **1996**, *92*, 4717.
(103) Yoon, C.; Yang, M. X.; Somorjai, G. A. *J. Catal.* **1998**, *176*, 35.
(104) Davis, S. M.; Somorjai, G. A. In *The Chemical Physics of Solid Surfaces and Heterogeneous Catalysis*; King, D. A., Woodruff, D. P., Eds.; Elsevier: Amsterdam, 1984; Vol. 4, Chapter 7.
(105) Henn, F. C.; Diaz, A. L.; Bussell, M. E.; Hugenschmidt, M. B.; Domagala, M. E.; Campbell, C. T. *J. Phys. Chem.* **1992**, *96*, 5965.
(106) Tsai, M. C.; Friend, C. M.; Muetterties, E. L. *J. Am. Chem. Soc.* **1982**, *104*, 2539.
(107) Firment, L. E.; Somorjai, G. A. *J. Chem. Phys.* **1977**, *66*, 2901.
(108) Smith, C. E.; Biberian, J. P.; Somorjai, G. A. *J. Catal.* **1979**, *57*, 426.
(109) Rodriguez, J. A.; Campbell, C. T. *J. Phys. Chem.* **1989**, *93*, 826.
(110) Demuth, J. E.; Ibach, H.; Lehwald, S. *Phys. Rev. Lett* **1978**, *40*, 1044.
(111) Petettiette-Hall, C. L.; Land, D. P.; McIver, R. T.; Hemminger, J. C. *J. Am. Chem. Soc.* **1991**, *113*, 2755.
(112) Peck, J. W.; Koel, B. E. *J. Am. Chem. Soc.* **1996**, *118*, 2708.
(113) Martin, R.; Gardner, P.; Tueshaus, M.; Bonev, C.; Bradshaw, A. M.; Jones, T. S. *J. Electron Spectrosc. Relat. Phenom.* **1990**, *54/55*, 773.
(114) Land, D. P.; Erley, W.; Ibach, H. *Surf. Sci.* **1993**, *289*, 237.
(115) Su, X. C.; Shen, Y. R.; Somorjai, G. A. *Chem. Phys. Lett* **1997**, *280*, 302.
(116) Neto, N. *Spectrochim. Acta* **1967**, *23A*, 1763.
(117) Lespade, L.; Rodin, S.; Cavagnat, D.; Abbate, S. *J. Phys. Chem.* **1993**, *97*, 6134.
(118) Haines, J.; Gilson, D. F. R. *J. Phys. Chem.* **1990**, *94*, 4712.
(119) Caillod, J.; Saur, O.; Lavalley, J.-C. *Spectrochim. Acta* **1980**, *36A*, 185.
(120) Dignam, M. J.; Moskovits, M.; Stobie, R. W. *Trans. Faraday Soc.* **1971**, *67*, 3306.
(121) Pearce, H. A.; Sheppard, N. *Surf. Sci.* **1976**, *59*, 205.
(122) Cremer, P. S.; Su, X.; Shen, Y. R.; Somorjai, G. A. *J. Phys. Chem.* **1997**, *101*, 6474.
(123) Carreira, L. A.; Carter, R. O.; Durig, J. R. *J. Chem. Phys.* **1973**, *59*, 812.
(124) Stidham, H. D. *Spectrochim. Acta* **1965**, *21*, 23.
(125) Hugenschmidt, M. B.; Diaz, A. L.; Campbell, C. T. *J. Phys. Chem.* **1992**, *96*, 5974.
(126) Campbell, J. M.; Seimanides, S.; Campbell, C. T. *J. Phys. Chem.* **1989**, *93*, 815.
(127) Segal, E.; Madon, R. J.; Boudart, M. *J. Catal.* **1978**, *52*, 45.
(128) Somorjai, G. A. *Surf. Sci.* **1995**, *335*, 10.
(129) Zhang, D.; Ward, R. S.; Shen, Y. R.; Somorjai, G. A. *J. Phys. Chem. B* **1997**, *101*, 9060.